Chem Soc Rev

TUTORIAL REVIEW

View Article Online
View Journal | View Issue

Cite this: *Chem. Soc. Rev.*, 2023, **52**, 6892

Tools to enable the study and translation of supramolecular amphiphiles

Thomas Allam,[a] Dominick E. Balderston,[b] Mandeep K. Chahal,[b] Kira L. F. Hilton,[b] Charlotte K. Hind,[c] Olivia B. Keers,[b] Rebecca J. Lilley,[b] Chandni Manwani,[b] Alix Overton,[b] Precious I. A. Popoola,[b] Lisa R. Thompson,[b] Lisa J. White[b] and Jennifer R. Hiscock *[b]

This tutorial review focuses on providing a summary of the key techniques used for the characterisation of supramolecular amphiphiles and their self-assembled aggregates; from the understanding of low-level molecular interactions, to materials analysis, use of data to support computer-aided molecular design and finally, the translation of this class of compounds for real world application, specifically within the clinical setting. We highlight the common methodologies used for the study of traditional amphiphiles and build to provide specific examples that enable the study of specialist supramolecular systems. This includes the use of nuclear magnetic resonance spectroscopy, mass spectrometry, X-ray scattering techniques (small- and wide-angle X-ray scattering and single crystal X-ray diffraction), critical aggregation (or micelle) concentration determination methodologies, machine learning, and various microscopy techniques. Furthermore, this review provides guidance for working with supramolecular amphiphiles in *in vitro* and *in vivo* settings, as well as the use of accessible software programs, to facilitate screening and selection of druggable molecules. Each section provides: a methodology overview – information that may be derived from the use of the methodology described; a case study – examples for the application of these methodologies; and a summary section – providing methodology specific benefits, limitations and future applications.

Received 19th June 2023

DOI: 10.1039/d3cs00480e

rsc.li/chem-soc-rev

Key learning points

(1) Key characterisation techniques used for the study of supramolecular amphiphiles.
(2) Benefits and limitations of different methodologies used in the study of supramolecular amphiphiles.
(3) The complimentary use of methodologies to enable extensive characterisation of supramolecular amphiphile systems.
(4) Gaining an understanding of supramolecular amphiphiles for translation into the clinic, the use of accessible online tools, and machine learning methods to aid rational design of drug-like molecules.
(5) Use of our flow chart tool to support the full characterisation of supramolecular amphiphiles and the higher-order structures produced through their self-assembly.

1. Introduction

Amphiphiles are molecules possessing both hydrophilic and hydrophobic components, typically a hydrophilic head and hydrophobic tail, that are traditionally held together through covalent bonding. Due to this combination of hydrophobic and hydrophilic properties, members from this class of compound can self-associate in solution to form a variety of morphologies, including micelles, vesicles, nanotubes, bilayers, tubules, and reverse micelles.[1] The importance of these amphiphilic systems is highlighted by their wide range of uses including, but not limited to, therapeutic applications (anticancer[2,3] or antimicrobial[3] agents and drug delivery systems),[4] material applications (functional biomaterials)[5] and as sensors or probes.[6] These amphiphilic morphologies possess characteristics that can be investigated using an extensive range of techniques, as outlined in Fig. 1. For example, techniques that are used to characterise amphiphiles include dynamic light scattering

[a] *School of Chemistry, University of Southampton, University Road, Southampton, SO17 1BJ, UK*
[b] *School of Chemistry and Forensic Science, University of Kent, Canterbury, CT2 7NH, UK. E-mail: J.R.Hiscock@kent.ac.uk*
[c] *Research and Evaluation, UKHSA, Porton Down, Salisbury SP4 0JG, UK*

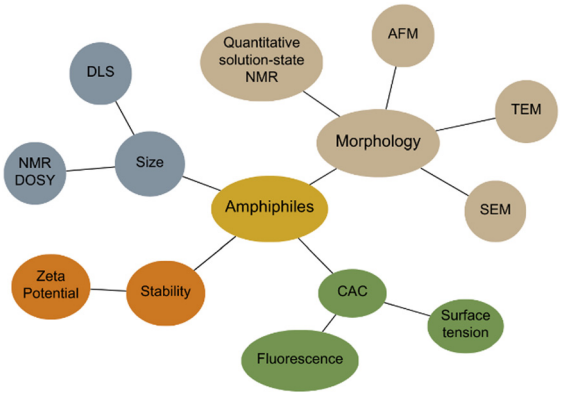

Fig. 1 Traditional techniques used in the characterisation of amphiphilic systems. Beige = morphology, blue = size, orange = stability, green = CAC determination.

(DLS)[7] and zeta potential,[8] which calculate the hydrodynamic diameter (d_H) and stability of the self-associated species produced respectively. In addition, diffusion ordered spectroscopy (DOSY) determines the d_H of low-order self-associated and individual molecular species through the attainment of individual resonance diffusion coefficients, which are applied to the Stokes–Einstein equation.[9–11] Furthermore, a range of techniques can be used to study the morphology of the higher-ordered self-associated structures that are formed, such as: atomic force microscopy (AFM);[12] transition electron microscopy (TEM);[13] scanning electron microscopy (SEM);[14] quantitative nuclear magnetic resonance (NMR) spectroscopy;[15] and ultraviolet-visible (UV-Vis) spectroscopy.[16] Defined as chemistry beyond the molecule, supramolecular chemistry is the study of the complex and organised molecular systems that form due to reversible non-covalent interactions, such as hydrogen bonding, in and/or between molecules.[17,18] Building on the traditional amphiphile, supramolecular chemists have developed the supramolecular amphiphile, or supra-amphiphile. This amphiphile sub-class utilises dynamic non-covalent interactions to help drive the formation of and/or stabilise amphiphile self-association events. In addition, these controllable self-assembly and disassembly events also enable the resultant higher-order structures produced to be effectively tailored towards a specific use.[1,19]

In addition, the incorporation of metals into higher-order structures produced through the self-assembly of these amphiphilic systems has been shown to result in the production of novel soft materials. These systems combine the advantages of amphiphilicity, such as self-assembly and biocompatibility, with that of adding metal-containing units, introducing biomolecular sensing[20] and magnetic properties[21] among others.

The aim of this tutorial review is to provide a single repository of information that enables the effective characterisation of supramolecular amphiphile systems, drawing on real world examples provided by literature resources, as summarised in Fig. 2. This review explores the use of NMR spectroscopy; mass spectrometry; X-ray scattering techniques, such as small- and wide-angle X-ray scattering (SAXS/WAXS); single crystal X-ray diffraction (SC-XRD); calculation of the critical aggregate concentration (CAC – which includes critical micelle concentration, CMC); various microscopy techniques; and the characterisation of metallo-centered supramolecular amphiphiles. This review also details the considerations that should be accounted for when working with supramolecular

Top left to right: Jennifer Hiscock, Charlotte Hind, Mandeep Chahal, Kira Hilton, Alix Overton, Thomas Allam, Chandni Manwani.
Bottom left to right: Olivia Keers, Dominick Balderston, Precious Popoola, Lisa Thompson, Rebecca Lilley, Lisa White.

Thomas Allam, PhD student studying cheminformatics. Dominick Balderston, PhD student studying the development of fluorescent amphiphiles. Mandeep Chahal, lecturer in chemistry studying the development of tetrapyrrole macrocycles as functional materials. Kira Hilton, PhD student studying novel approaches to characterise molecular level interactions with biologically relevant membranes. Charlotte Hind, senior project team leader working to discover and develop novel antimicrobial therapies. Jennifer Hiscock, professor in supramolecular chemistry studying supramolecular self-associating amphiphiles. Olivia Keers, PhD student studying the development of synthetic molecules for intracellular targeting. Rebecca Lilley, PDRA investigating the effect of membrane composition on the cation transport activity of supramolecular amphiphiles. Chandni Manwani, PhD student in cancer biology. Alix Overton, PhD student studying the use of microfluidics for bacterial detection under flow. Precious Popoola, PhD student studying the development of supramolecular therapeutic agents. Lisa Thompson, Daphne Jackson Research Fellow studying the development of supramolecular amphiphiles for targeted drug delivery. Lisa White, PDRA exploring the potential for supramolecular self-associating amphiphiles to be developed as antimicrobial agents.

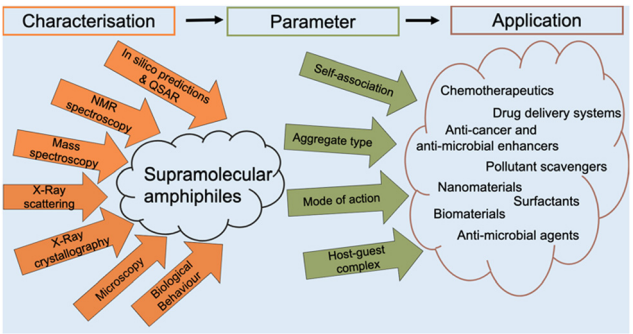

Fig. 2 Different techniques for characterising supramolecular amphiphiles (orange), the subsequent parameters obtained from the characterisation (green), and the various applications of supramolecular amphiphiles (brown).

amphiphiles in a biological setting, the use of *in silico* property prediction models and computational quantitative structural activity relationship (QSAR) techniques. Each of the 10 sections of this review features a brief description of the technique and how it is used followed by a case study drawing on literature examples. To avoid duplication of resources, complimentary reviews and other publications have been signposted where necessary.

From our work in this area, we believe that there is a gap in the literature regarding processes to enable the full and effective characterisation of supramolecular amphiphiles and the supramolecular structures they form due to their unique nature. This review aims to begin to fulfil this unmet need and to highlight where novel innovation in this area may be required, inspiring and supporting others already working within, or with a desire to enter this sub-field of supramolecular chemistry. Figures and Tables have been colour shaded where possible to aid visual accessibility for the reader, unless this process was found to interfere with image clarity.

2. Discussion

2.1 Nuclear magnetic resonance (NMR) spectroscopy

Advances in NMR spectroscopy, combined with the large range of NMR spectroscopy active nuclei available for study, have resulted in this apparatus becoming one of the most powerful and versatile tools for use in the field of supramolecular chemistry and beyond. NMR spectroscopy is primarily used to identify and quantify molecular structure and intra- or intermolecular interaction information of both pure and complex mixtures, in either the solid,[22,23] semi-solid[24] or solution state.[25,26]

NMR spectroscopy reports on the electronic environment of the nuclei under investigation. This may be affected by multiple factors, which include the presence of conjugation; the proximity of neighbouring covalently bound elements (functional groups); the presence or formation of intra- or intermolecular interactions. The slower tumbling rate of larger aggregated species can also lead to difficulties in observing these systems using conventional solution-state NMR spectroscopy. A slower tumbling rate leads to signal broadening, which complicates or prevents accurate spectral analysis.[27] As a result, this technique is often used to characterise non-covalent complexation events.[28,29]

High-resolution magic angle spinning (HR-MAS) NMR spectroscopy utilises a combination of solid- and solution-state NMR spectroscopy techniques, enabling the spectra of semi-solid samples, which have restricted molecular mobility, to be obtained using a solution-state NMR spectrometer to run standard solution-state experiments.[30] This non-destructive method is routinely used to analyse both amorphous crystalline and gel-like materials. The collection of high-resolution data is enabled by rapid specimen uniaxial rotation, which is inclined at 54° – the magic angle.[31]

Solid-state NMR spectroscopy is routinely used for the generation of high-resolution structures of protein aggregates, crystallised proteins, and membrane proteins.[32] In addition, solid-state NMR spectroscopy has also been used to investigate the non-covalent interactions contained within model phospholipid (an amphiphilic species) bilayers which contain naturally abundant NMR active nuclei, ^{31}P (100%) and ^{14}N (99.63%).[33]

Through comparative integration of the molecular signal to that of a known internal standard, quantitative solution-state ^{1}H NMR spectroscopy (qNMR) studies allow for the elucidation of any non-detectable (due to the size and limitations of the spectrometer), higher-order structures that may be present in a specific solvent environment.[34] In addition to one-dimensional NMR spectroscopy, complimentary two-dimensional (2D) NMR spectroscopy techniques are also useful for structural determination, such as correlation spectroscopies (COSY and TOCSY), nuclear Overhauser effect spectroscopy (NOESY) and rotating-frame nuclear Overhauser effect spectroscopy (ROSEY),[35] and DOSY, as described within the introduction section of this review.[9–11]

Supramolecular amphiphiles incorporate additional non-covalent interactions to stabilise any resultant aggregate structure formed. Therefore, to fully characterise these systems, the strength of these molecular level association events needs to be quantified. Methods to enable the quantification of these interactions are provided within the case study 1a.

Although common for standard molecular structural characterisation, this simple technique is not frequently used for amphiphilic self-association constant determination, with only a limited number of examples reported within the literature.[36,37] Furthermore, molecular association events have to be observed below CAC, meaning that determining these values at lower concentrations through the use of UV-Vis spectroscopy or fluorescence may be more appropriate. However, these aforementioned methods do not give as much detailed information as ^{1}H NMR spectroscopy, where the formation of any hydrogen bonds can be directly observed through monitoring the change in chemical shift of a specific resonance, upon change in the concentration of the amphiphile (self-association) or guest (host–guest complex formation).

There are two types of molecular association events typically of interest to those working in the field of supramolecular

amphiphiles: (i) those that involve a single chemical species and undergo self-associative complexation events, and (ii) those that involve more than one molecular species, therefore undergo host–guest complexation. The strength of interaction between the molecular species involved in these events is reported, either as an association constant, or the corresponding dissociation constant.

Thordarson and co-workers have produced several very useful reviews explaining the concepts behind the calculation of these values for these different complexation events, so further discussion is not provided here.[38,39] In addition, these field experts have produced a freely accessible online tool (BindFit)[40] to enable calculation of various molecular association constants from not only NMR spectroscopy data, but also UV-Vis or fluorescence data. Self-associative binding constants are produced through dilution studies, in which a concentrated sample of the compound being investigated undergoes serial dilution at or below CAC in the case of amphiphilic compounds. However, association constants calculated from heterogeneous complexation events require titration experiments to be performed again at or below CAC, in the case of amphiphilic compounds, where the concentration of the 'host' is kept the same and the concentration of the 'guest' is systematically increased, usually until 6–10 molecular equivalents of the guest have been added. Upon the formation of any intermolecular interactions, a comparative change in the electronic environment of those nuclei directly involved with or in close proximity to the complex formation event is apparent. The change in chemical shift values are then fitted to a binding isotherm model that allows for elucidation of any corresponding self-associative binding constants.[36,37,41]

The two most widely utilised single self-associative binding models applicable here are the co-operative equal K (CoEK) model, which assumes the first association event is different from all subsequent identical association events,[42] and the dimerisation/equal K (EK) model, where all association events are equal. Here both models assume one component, unidirectional homogenous aggregation events.[43]

Case study 1a. Hydrogen bond donating (HBD) receptors for the selective coordination of anionic guest species in competitive solvent mixtures are well recognised in the field of supramolecular chemistry.[44,45] Comparatively, there are far fewer examples of low molecular weight compounds ($M_W < 500$) which contain HBD units covalently linked to an anionic hydrogen bond accepting (HBA) substituent.[46] Exploring this void in the field of supramolecular chemistry, Hiscock and co-workers developed a series of structurally related supramolecular self-associating amphiphiles (SSAs) incorporating the (thio)urea-alkyl spacer-anion motif within the modular molecular SSA skeleton (Fig. 3A).

To gain an insight into any self-association processes in the solution-state, preliminary DLS studies were performed for **1–5** (Fig. 3B) in competitive solvent systems, ranging from mostly aqueous systems through to 100% DMSO. The data generated showed the presence of higher-order structures with a $d_H >$ 100 nm in an aqueous environment. However, in a 100% DMSO solution, molecular structures with a $d_H \approx 1$ nm were recorded, hypothesised to be lower-order monomeric or dimeric species. To support this hypothesis a series of 2D ^{1}H NMR DOSY spectroscopy experiments were conducted in DMSO-d_6-0.5% H_2O. The resonance diffusion coefficients were applied to the Stokes–Einstein equation, where a d_H of $\approx$ 1.6 nm was generated for the anionic component of the compound, corroborating with those results from the DLS studies.[11]

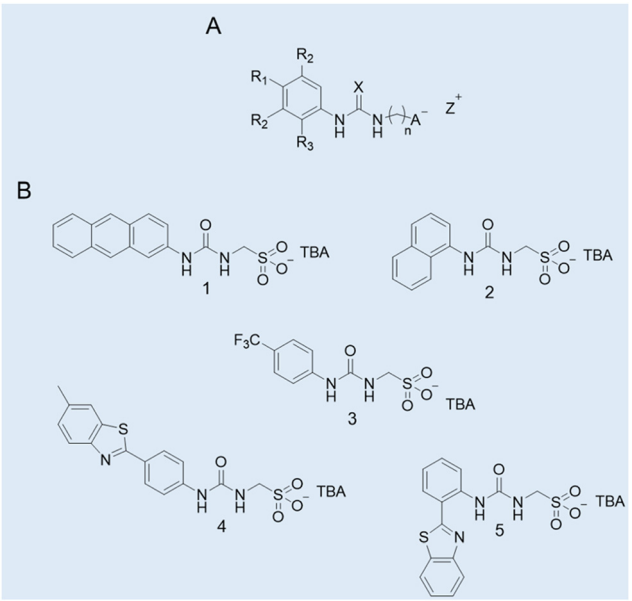

Fig. 3 (A) General chemical structure of an SSA. R = any group; X = S or O; n = 1, 2, or 3; A^- = sulfonate or carboxylate; Z^+ = counter cation. (B) Molecular structures of SSAs developed by Hiscock and co-workers (**1–5**).[11] TBA = tetrabutylammonium. Reproduced/adapted from ref. 11 with permission from RSC *Chemical Science*.

To gain a quantitative understanding of the molecular self-association interactions of those lower-order complexation events, a series of ^{1}H NMR spectroscopy dilution studies were performed in DMSO-d_6-0.5% H_2O. The downfield changes in chemical shift of the corresponding HBD N–H resonances with increasing concentration were monitored, and these data were then fitted to both the EK and CoEK binding isotherm models using BindFit, Table 1.

Comparative analyses of those values obtained show the EK model (K_{dim} values) to give the best fit for those data obtained,

Table 1 Overview of self-association constants (M^{-1}) calculated from the fitting of ^{1}H NMR spectroscopy dilution data and refined to the EK and CoEK binding isotherm models for SSAs **1–5** in a DMSO-d_6-0.5% H_2O solution at 298 K. Error displayed as a percentage of the calculated value

	EK model (M^{-1})		CoEK model (M^{-1})		
SSA	K_e	K_{dim}	K_e	K_{dim}	p
1	2.9 ± 0.5	1.5 ± 0.2	8.6 ± 1.1	4.3 ± 0.5	0.5 ± 2.5
2	<0.1 ± 1.5	<0.1 ± 0.8	0.5 ± 43.1	0.3 ± 21.5	0.0 ± 47.0
3	0.6 ± 3.0	0.3 ± 1.5	13.0 ± 5.7	6.5 ± 2.9	0.2 ± 23.8
4	5.3 ± 0.6	2.7 ± 0.3	13.0 ± 0.7	6.5 ± 0.3	0.5 ± 2.0
5	1.2 ± 2.1	0.6 ± 1.1	6.2 ± 8.8	3.1 ± 4.4	0.4 ± 17.8

thus providing further evidence towards the presence of hydrogen bonded dimeric species in solution. Furthermore, a correlation was determined between the inverse of the calculated self-association constants and nanostructure d_H determined from analogous DLS studies, where smaller self-associated aggregates exhibited stronger self-associative interactions.[11]

In subsequent studies, the authors have continued to utilise this technique, applying it to their extensive library of SSAs in order to investigate any self-associative complexation events.[15,34,36,37,47,48]

Summary

This work highlights the use of NMR spectroscopy as a non-destructive, accessible, *in situ* tool, offering unique insight towards the quantification of molecular level association events for supramolecular amphiphiles. Further advantages include a large temperature range (−150 °C to 150 °C) and multiple state analysis (semi-solid, solid and solution). Furthermore, NMR spectroscopy allows for the elucidation of solution-state non-covalent interactions of both pure and complex mixtures, with complimentary, freely available, simple to use, BindFit software allowing for the derivation of self-association constants and host–guest complexation events.

Limitations

As a characterisation tool, there is difficulty in spectral analysis of high molecular weight complex mixtures due to a greater potential for signal overlap. For association constant quantification using BindFit, the isotherm models are limited to either 1 : 2 or 2 : 1 for host–guest complexation events, and homogenous (1 : 1) unidirectional polymerisation events for self-association constant derivation.

2.2 Mass spectrometry (MS)

The continued development of mass spectrometry (MS) methodologies and equipment has resulted in the development of high-resolution mass spectrometry (HRMS) which can determine the difference in mass of two compounds by as little as ±0.0001 Da.[49] Examples of HRMS methodologies include, time of flight (ToF) MS, orbitrap MS and Fourier-transform ion cyclotron resonance (FT-ICR) MS.[50]

There are multiple examples for the use of MS (sometimes used in combination with ion mobility spectrometry) for characterisation of supramolecular assemblies and amphiphiles throughout literature.[51–54] The most common use of this technique within the field of chemistry is the determination of the *m*/*z* for a single molecule. However, there has always been a desire to develop HRMS methodologies to characterise non-covalent interactions and subsequent molecular morphologies. The most substantial advancement in MS, which has allowed the characterisation of supramolecular molecules in general, is the development of soft ionisation techniques. Examples include fast atom bombardment (FAB), matrix-assisted laser desorption ionisation (MALDI), and electrospray ionisation (ESI).[55] Soft ionisation is a low energy approach to form charged species, resulting in reduced molecular and complex fragmentation events and maintenance of the parent ion, thus enabling the study of less robust molecules such as proteins, DNA, and supramolecular structures.[55]

A common use of MS for the study of supramolecular amphiphiles, in addition to the characterisation of the monomeric species in line with standard molecular characterisation methodologies, is the characterisation of intermolecular association events. For example, Stoikov and co-workers have used MALDI-ToF MS to demonstrate the self-assembly of amphiphilic *p-tert*-butylthiacalix[4]arenes based derivatives in the presence of water-soluble nanoparticles.[56] The following case studies show two crucial methodologies for HRMS characterisation of amphiphiles.

Case study 2a. Perylene tetracarboxylic diimide (PDI) exhibits photo- and electro-properties, such as high charge carrier mobility and high fluorescent quantum efficiency. PDI has strong π–π interactions forming self-assembling motifs which, in the solid-state, limit quantum efficiency and therefore practical applications. Zhu and co-workers hypothesised that by increasing molecular complexity of PDI, for example by incorporating isobutyl-functionalised polyhedral oligomeric silsesquioxanes (BPOSS) and fullerene (C_{60}), the synthesised shape amphiphile could display varying properties depending on self-assembled morphology, binding mode and quantum efficiency.[57] Travelling wave ion mobility mass spectrometry (TWIM-MS) was utilised in combination with collision activated dissociation (CAD) within the quadrupole ToF MS. Within the CAD experiment, drift gas collides with the ionic species causing any self-associated species to dissociate; the energy required to overcome these supramolecular interactions is then determined. Altering electric field, gas flow, shape, and net charge influences the mobility of the ions within the experiment, in this case resulting in identification of the monomer, dimer and trimer self-associated complexes. PDI self-assembles through π–π stacking, while the POSS and C_{60} units increase steric bulk, thus influencing the molecular packing arrangement. Utilising complimentary ESI-TWIM-MS with CAD allowed not only the identification of the monomeric and dimeric species, but also variation in the assembly of the dimeric species through identification of differences in strength of their non-covalent interactions, Fig. 4.[57]

Analysis of these dimers with TWIM-MS can be used to indicate how changes in molecular binding mode may alter quantum efficiency and subsequent photo- and/or electro-properties of aggregation induced emission (AIE) events.[58] While HRMS provides data relating to the non-covalent binding mode in only the gas-phase. ESI-TWIM-quadrupole-ToF-MS provides data enabling not only the identification of the formation of monomers, dimers, trimers, and oligomers, but also provides insight into complex variation and stability. It should be noted that full characterisation of any non-covalent complex formation events requires additional complementary techniques in multiple phases, such as solid-state SC-XRD or solution-state NMR spectroscopy and CAC determination.

Case study 2b. SSAs, patented by Hiscock and co-workers, are a class of >50 structurally related chemical compounds (Fig. 3). In general, SSAs have been shown to form anionic

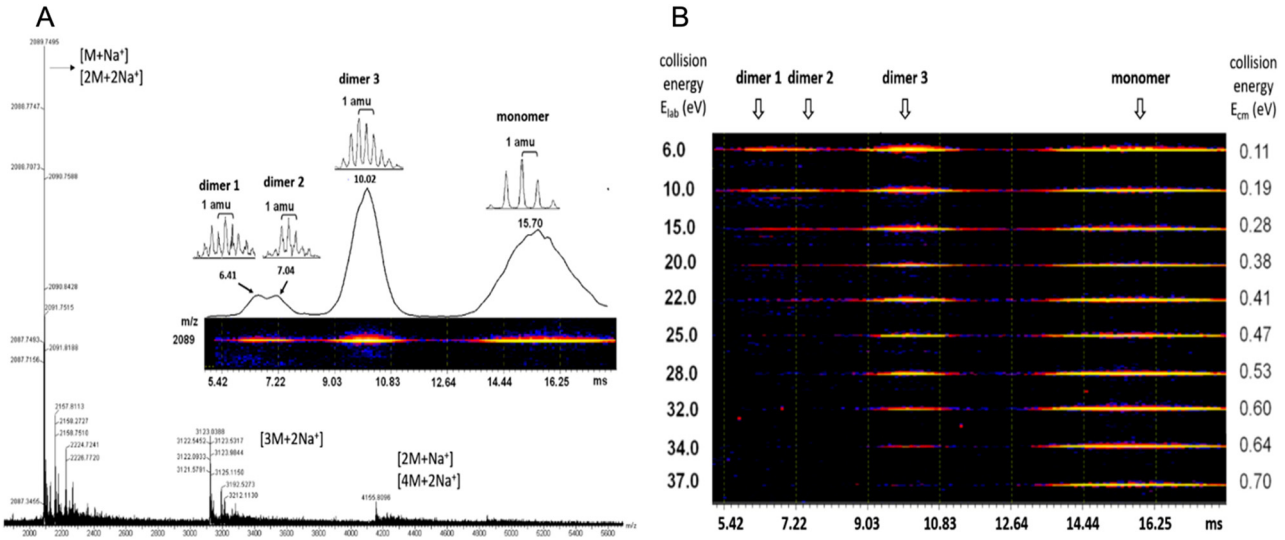

Fig. 4 (A) ESI MS of (BPOSS-PDI-C_{60}). (B) 2D TWIM-MS plot of dimer and monomers present and their dissociation energies. Reproduced/adapted from ref. 57 with permission from MDPI *Molecules*.

hydrogen bonded dimers in organic polar solvents such as DMSO, spherical aggregates ($d_H \approx$ 100–550 nm in aqueous conditions) and, in some instances, to form gel fibres upon the addition of certain salts, following an annealing process.[5,15] However to support that lower-order structures formed by this class of compounds in polar organic solvents were likely to be dimers of the SSA anionic component, HRMS-ESI$^-$ methodologies were utilised to confirm those self-associated species present in the gas-phase.[11] This study showed that a high percentage of those SSAs tested (Fig. 3B) existed as dimeric species in the gas phase, exemplified in Table 2.

The self-associated SSA anionic species observed in polar organic solvents, hypothesised to be hydrogen bonded dimers, were generally shown to persist in the gas phase. However, when comparing the results from the two benzothiazole substituted SSAs **4** and **5**, Table 2 and Fig. 3, anionic dimers were not observed for **5**. SC-XRD of the anionic component of **5** showed the formation of a competitive intramolecular bond between the urea NH group and the nitrogen contained within the benzothiazole functionality, hypothesised to comparatively weaken any SSA anion intermolecular self-association complex formation. In addition, calculation of the dimerisation constant for the anionic component of **4** and **5** in DMSO-d_6-0.5% H_2O confirmed the strength of hydrogen bonding self-association to be stronger for **4** over **5**, 2.7 M^{-1} and 0.6 M^{-1} respectively. This provided further evidence for the presence of an intramolecular hydrogen bond within **5**, weakening any potential hydrogen bonding self-association events.[11] The increased strength of SSA anion hydrogen bond formation has also been correlated to a decrease in CAC. Therefore, HRMS supports data collected from both solution and solid-state studies.

Table 2 Experimentally derived *m*/*z* values of monomeric and dimeric species present under HRMS-ESI$^-$

	m/*z* $[M]^-$		*m*/*z* $[M + M + H^+]^-$	
SSA	Theoretical	Actual	Theoretical	Actual
1	329.0602	329.0567	659.1204	659.1210
2	279.0445	278.9615	559.0890	556.9373
3	229.0289	229.0292	459.0578	459.0649
4	376.0431	376.039	753.0862	753.0864
5	362.0275	362.0261	Not observed	

Summary

Due to the development of soft ionisation techniques, HRMS-ESI and TWIM-MS are viable methodologies to study the assembly of supramolecular amphiphiles. This methodology, although destructive, requires one of the lowest sample sizes (<1 mg) for effective analysis of those methods discussed herein. While further distinguishing between non-covalent arrangements in the gas phase provides insights into mechanism of functional properties, this methodology requires additional analytical techniques in tandem. Therefore, HRMS is best served as a key fragment in addition to other characterisation methods.

Limitations

The aggregates formed through supramolecular amphiphile self-assembly processes are often reliant on the solvent environment present, which limits the application of this gas-phase technique towards the study of these systems. MS is a destructive technique and often requires additional techniques to support any observations made.

2.3 X-Ray scattering techniques

X-Ray scattering techniques have been used to analyse many different types of structures produced through a variety of molecular self-association events, from crystalline materials to polymers, and biological macromolecules. The resulting data provides valuable information, from general structural information to material morphology[59] and details relating to the material swelling process.[60]

Of the multiple X-ray scattering techniques available, there are two of direct interest to those studying supramolecular amphiphiles: SAXS, and WAXS (also known as SAXD and WAXD). SAXS is used to analyse non-crystalline materials, whereby WAXS is used for analysing crystalline materials. This is advantageous when characterising those materials produced through the assembly of supramolecular amphiphiles that form amorphous aggregates that are not crystalline by nature or cannot be readily crystallised. In general, SAXS and WAXS are non-destructive techniques that can be used on a variety of sample types including, but not limited to, solids, powders, gels, and liquids. However, some solid materials, which are typically run on sample plates requiring around 5 μL of each material, may also require the use of capillary tubes. Depending on the specific instrument used and experimental set-up, a sample volume of 50–200 μL is required. SAXS typically scatters X-rays at small angles ($<5^\circ$), while WAXS scatters X-rays of $>5^\circ$. This difference in angle has a major impact on the information that is obtained. SAXS produces information relating to the dynamics and molecular structure of the sample (1–100 nm), whilst WAXS provides details of the sub-nanometre structures (0.2–1 nm), such as the crystal lattice and unit cell dimensions. While these methods are used to obtain specific structural data, they are often used in conjunction with additional techniques to allow full characterisation of a sample. These techniques can include but are not limited to NMR spectroscopy,[61] differential scanning calorimetry (DSC),[62] TEM,[63,64] AFM, SEM and Raman spectroscopy.[65]

Case study 3a. This case study, produced by Lin and co-workers, focuses on the use of WAXS to characterise supramolecular amphiphile systems.[63] Within this featured example, the asymmetric giant amphiphile, diBPOSS-C_{60} (**6**, composed of two polyhedral oligomeric silsesquioxanes with isobutyl surface groups, BPOSS and one C_{60}, Fig. 5), was characterised using several techniques including WAXS. Here, temperature dependent WAXS was used to study the phase behaviour and the structural development of diBPOSS-C_{60}.

Initial DSC measurements, between 0 °C and 240 °C, were carried out to determine the melting and crystallisation behaviour of diBPOSS-C_{60}. Initially, the sample was heated to 240 °C, before being cooled to 0 °C at a rate of −10 °C min^{-1}, followed by the second heating run at 10 °C min^{-1}. The results of this study found several endothermic processes, between 165 °C and 200 °C, that were hypothesised to be due to either the melting of a singular crystal form with different stabilities, or multiple crystal forms with individual melting points. The data obtained from DSC measurements alone identified these anomalies but were not able to ascertain their source. Therefore, temperature dependent WAXS was employed using analogous experimental parameters.

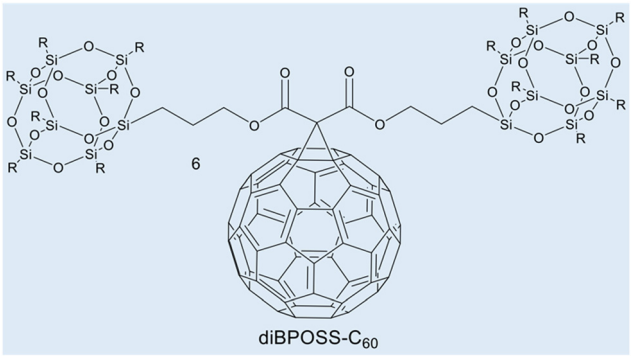

Fig. 5 Chemical structure of diBPOSS-C_{60} **6**. Reproduced/adapted from ref. 63 with permission from Elsevier *Polymer*.

At 30 °C, amorphous halo peaks were present at $2\theta \approx 2.8^\circ$, 9°, and 19°. As the temperature increase continued to 110 °C, diffraction peaks started to appear. The peaks became more distinguishable with increased intensity as the temperature rose to 190 °C, however, they did not change position. At 200 °C, the diffraction peaks disappeared, and the amorphous halo peaks returned, showing the structure met its isotropic melting point.

These WAXS data showed that the endothermic peaks in the DSC scan were due to one crystalline structure with varying sizes, formed with thermal annealing, and therefore with different stabilities. The information provided from the WAXS experiment was also combined with selected area electron diffraction (SAED). Analysis of these data confirmed the unit cell as orthorhombic. The resulting asymmetric supramolecular amphiphile structure was found to consist of a single C_{60} layer sandwiched between two BPOSS layers.

Case study 3b. In the following example, Pradham and co-workers synthesised three phenylalanine-derived amphiphiles (PDAs), NapF-DETA, NapF-EDEA and NapF-TREN.[61] Other examples for the use of SAXS to characterise alternative supramolecular systems have also been produced.[66,67] The aim of this work was to create three anion and pH responsive supramolecular hydrogels from these PDAs, for use as sequential drug release systems. TEM confirmed all three PDAs to form fibrillar structures upon self-assembly in water. Hydrogels of these materials were produced using the heat/cool method, at an amphiphile concentration of 10 mg mL^{-1}. Excitingly, NapF-TREN retained a self-supporting hydrogel post syringe extrusion. Upon addition of $H_2PO_4^-$ and HSO_4^-, supplied as the sodium salt, hydrogels formed from NapF–TREN showed a rapid response in the form of a gel–sol transition. This response was examined further using circular dichroism (CD), TEM, AFM, NMR spectroscopy and SAXS. SAXS allowed the material to be studied in the solution phase, removing the possibility of artifacts produced through sample dehydration. SAXS data obtained from the NapF-TREN hydrogel, in the presence and absence of additional salts, was and subsequently fitted to the Porod cylinder model. This resulted in the identification of nanofiber diameters ≈15 nm however, upon the addition of NaCl the diameter of fibres was found to reduce to ≈7.9 nm (Fig. 6A).

Upon the addition of HSO_4^- and $H_2PO_4^-$ to the NapF-TREN hydrogel, triggering the gel–sol transition, the SAXS data was fitted to a sphere model. Here particle diameters of ≈7–10 nm were identified, supporting results obtained from complimentary TEM and AFM studies. However, after two days

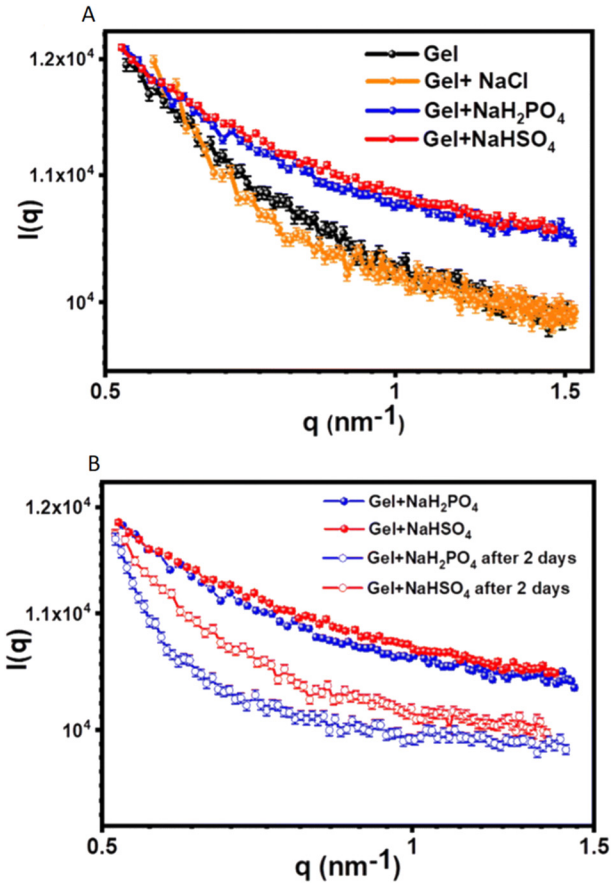

Fig. 6 SAXS scattering plots produced from the analysis of the NapF-TREN hydrogel: (A) before and after the addition of Cl^-, $H_2PO_4^-$ and HSO_4^- ions, supplied as the sodium salt; (B) showing the effect of material ageing. Reproduced/adapted from ref. 61 with permission from RSC *Nanoscale*.

of material ageing (Fig. 6B), SAXS data confirmed the reformation of nanofibers with a diameter of ≈7 nm. This anion responsive hydrogel was then subsequently tested to confirm an additional pH response in order to verify the materials potential for development as a sequential drug release system. As a proof of concept, therapeutic agents propranolol and doxorubicin were first entrapped within the hydrogel. The initial addition of NaH_2PO_4 was shown to release propranolol, this was followed by a change in pH, which triggered the subsequent release of doxorubicin.

Summary

WAXS is a non-destructive, high throughput technique, which can be used on several forms of materials requiring sample sizes <200 μL. Depending on the sample that is to be analysed, WAXS and SAXS, can be carried out in the laboratory using accessible benchtop equipment.

Case study 3a shows temperature dependent WAXS to be a useful tool for the analysis of crystalline materials composed of supramolecular amphiphiles, characterising phase behaviour and structural changes.

Case study 3b demonstrates the use of SAXS as a valuable method for analysing the morphology of amphiphilic systems in the solution-phase.

Limitations

WAXS can only be used on crystalline and semi-crystalline materials, as such, for supramolecular amphiphiles that do not readily crystallise, only SAXS may be accessible. For samples that are weakly scattering, specialist beam lines with high intensity X-rays are also required.

2.4 Single crystal X-ray diffraction (SC-XRD)

SC-XRD is a non-destructive solid-state technique used to determine the three-dimensional (3D) atomic arrangement of a molecule(s) in the solid-state for materials that exist as a single crystal.[68] This methodology enables the determination of the length and angle of a chemical bond present in the sample,[69] alongside interactions between atoms including non-covalent bonds such as hydrogen bonds[70,71] and π–π stacking.[72] Unlike X-ray scattering techniques, X-ray diffraction requires crystalline samples and a high energy X-ray source. SC-XRD measurements can be determined at a wide range of temperatures (80–400 K) and can distinguish between different polymorphs (a form of isomerism where the same material can form different crystal structures). Polymorphisms can cause differences in physical properties of the material, including hygroscopicity, density, and colour.[73] Understanding these differences can lead to the informed design of the material.[74] This technique is utilised in many different fields of chemistry, for example in macrocyclic supramolecular chemistry, where any self-assembly processes can be identified, and sizes of any supramolecular structures determined.[75]

Case study 4a. Haldar and co-workers utilised SC-XRD in their study characterising acid and thermal responsive supramolecular polymer gels.[76] The authors synthesised 7 (Fig. 7A), designed to be complimentary to the toroidal structure of cyclodextrin, resulting in the formation of a supramolecular polymer which, upon heating and cooling, formed a gel in a DMSO : H_2O (1 : 2) solution. Here, SC-XRD was used to characterise the self-assembled structures that exist in the crystalline solid state. Here, 7 formed parallel sheet-like structures (Fig. 7B), stabilised through the formation of hydrogen bonds between different molecules and π–π stacking utilising the phenyl ring systems. An extended structure was also observed, forming a corrugated sheet-like structure that was stabilised *via* dispersion forces between the caproic acid alkyl chains (Fig. 7C).

Summary

SC-XRD is a non-destructive technique which uses <5 mg of sample (depending on quality) whilst producing a substantial amount of data (including 3D positioning of the atoms in space and determination of polymorphisms) and operates at a wide range of temperatures. SC-XRD enables insight into the self-associative nature of amphiphiles in the solid state, which are often hypothesised to affect nanostructure and material formation.[5]

Limitations

Supramolecular amphiphiles may not readily crystallise and optically clear single crystals must be produced. Crystals should be between 50–250 μm in size. The information gathered is only

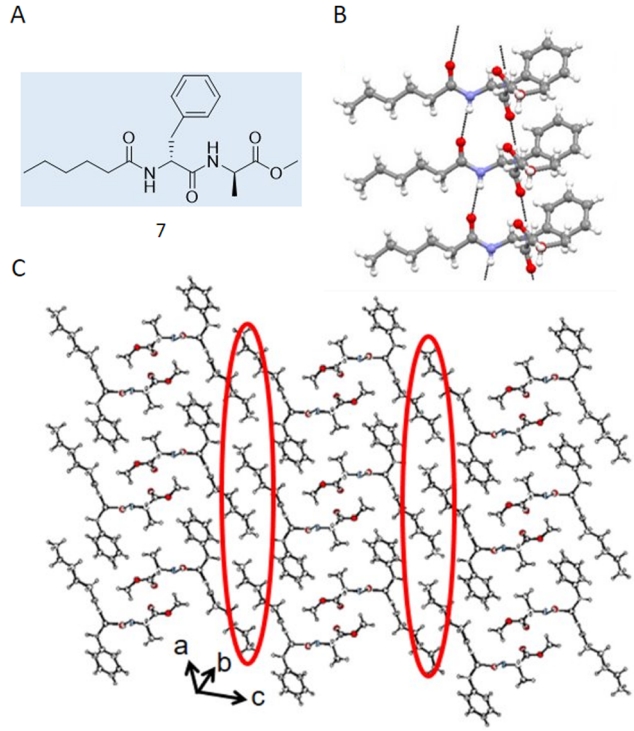

Fig. 7 (A) Chemical structure synthesised by Halder and co-workers **7**. (B) Crystal structure of **7** showing a hydrogen bonded sheet stabilised by π–π interactions. (C) Extended crystal structure, showing how hydrophobic interactions (circled in red) stabilise interactions between sheets. Carbon = grey, oxygen = red, nitrogen = blue, hydrogen = white. Reproduced/adapted from ref. 76 with permission from MDPI *Chemistry*.

applicable to solvent-free conditions when amphiphile self-assembly is influenced by solvent environment.[41]

2.5 Metallo-centred supramolecular amphiphiles

Characterisation of metallo-supramolecular self-assembled amphiphiles is typically realised employing conventional techniques used in their non-metallic counterparts. The list includes DLS, AFM, TEM, cryo-TEM, SEM, as well as NMR spectroscopy. These techniques have been discussed in the introduction and other sections of the review, and typically obtain information about the morphology and size distribution profile of those species present ($d_H \approx$ 0.5 nm to 2.5 μm). Besides conventional techniques, information on metallo-centred amphiphiles is expanded using other spectroscopy techniques such as UV-Vis, emission and ^{1}H NMR spectroscopy titrations.[77] Comparative UV-Vis and emission spectral data produced through titration experiments, analogous to those described within Section 1 of this review, enables identification of shifts in absorption peak maxima and/or appearance of new peaks due to charge-transfer between metal centre and amphiphile, indicating the formation of supramolecular aggregates[78] or transformations among different/discrete self-assembled states.[79] Furthermore, additional insight towards the role of metals in amphiphile aggregation has been achieved by using supplementary techniques such as analytical ultracentrifugation (AUC), CD, energy dispersive X-ray (EDX) spectroscopy, X-ray photoelectron (XPS) spectroscopy, as well as coupled plasma-atomic emission spectrometry (ICP-AES). EDX, XPS and ICP-AES can detect or confirm the presence of metals in self-assembled aggregates,[80,81] whereas AUC is used for the determination of micellar molar masses and d_H in the case of polymeric metallo-supramolecular assemblies. CD is used to study the chirality in supramolecular assemblies and gives information relating to dynamic behaviour under the influence of external stimuli, such as metal ions or pH. In this section of the review, we will discuss how these additional techniques are used to characterise and study metallo-supramolecular amphiphiles.

2.5.1 Analytical ultracentrifugation (AUC). AUC is a highly versatile analytical method used to study the behaviour of macromolecules, proteins, and polymer systems in solution under the influence of strong centrifugal forces.[82,83] Particles subjected to these forces undergo sedimentation processes that can be tracked in real time using UV-Vis optical systems. AUC offers several approaches for studying sedimentation processes. Observations of dynamic behaviour (sedimentation velocity) or equilibrium regimes (sedimentation equilibrium), can provide information about size, state of association in solution, density, and conformational changes of biological and other macromolecules.

In characterising polymeric metallo-supramolecular assemblies, use of AUC is preferred over DLS and static light scattering (SLS).[84] DLS and SLS give information about the diffusion coefficient, d_H, as well as the polydispersity of aggregated species. However, in the case of polymeric metallo-supramolecular assemblies, both of these methods suffer from limitations that include: the presence of large aggregates and lack of sample uniformity, which affect the measurements, such as scattering intensity (I), where $I \propto d^6$ (where d is a diameter of macromolecule), therefore unable to detect smaller particles; and strong absorption by metal aggregates complicates the interpretation of light scattering data. In contrast, for AUC, sedimentation velocity experiments can discriminate whether a sample is homogeneous in solution or a mixture of forms (*e.g.* monomer/dimer, or aggregates), and sedimentation equilibrium is particularly useful for determination of molecular weights of aggregated species or subunit stoichiometry (monomer, dimer, trimer *etc.*) in solution.

Case study 5a. Schubert and co-workers have developed a strategy for the construction of metal-based block copolymer architectures.[85] A metal–ligand complex is used as a supramolecular linker between the hydrophobic and hydrophilic blocks of the amphiphilic block copolymers, giving rise to a metallo-supramolecular block copolymer that forms micelles in aqueous solutions.[86] DLS and TEM were used for initial characterisation of the size and morphology of non-uniform aggregates (d_H = 65–202 nm).[87,88] Considering the drawbacks related to DLS for studying the heterogeneous samples (low resolution and unable to detect smaller particles), AUC was used to study the aggregation of metallo-copolymers in solution.[89] PS_{20}-[Ru]-PEO_{70} (**8**) and PS_{20}-[Ru]-PEO_{375} (**9**) copolymers were prepared by connecting two block copolymers, poly(styrene) segment and poly(ethylene oxide) block *via* a bis-(2,2′:6′,2″-terpyridine-ruthenium) unit (Fig. 8).[90]

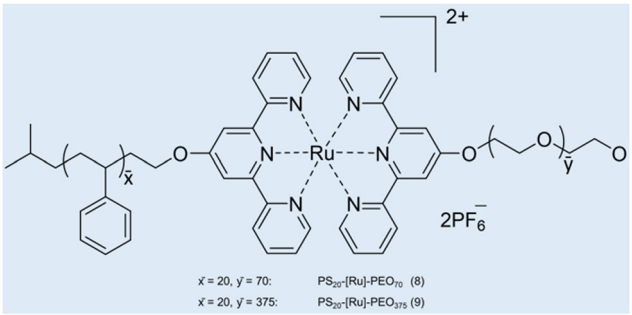

Fig. 8 Structures of the two micelle-forming copolymers PS_{20}-[Ru]-PEO_{70} **8** and PS_{20}-[Ru]-PEO_{375} **9**. Reproduced/adapted from ref. 90 with permission from the Wiley *Journal of Polymer Science Part A: Polymer Chemistry*.

Kinetically frozen micelles of **8** and **9** were prepared by adding water to the copolymer/DMF solution with a syringe pump, and equilibrium micelles of **9** were prepared by incubating in H_2O for 2–3 weeks. The resulting micelles were characterised by sedimentation velocity and sedimentation equilibrium analyses in an analytical ultracentrifuge and by TEM. Sedimentation analysis showed unimodal size distributions. Micelles of **8** were found to have an average molar mass (M) $\approx$ 318 000 g mol^{-1} (corresponding to 53 protomers per micelle) and $d_H \approx$ 18 nm, whereas micelles of **9** showed $M \approx$ 603 000 g mol^{-1} (31 protomers per micelle) and $d_H \approx$ 34 nm. However, the TEM results are different from the sedimentation analysis, mainly because of imperfections in the staining procedure as TEM on unstained samples emphasise on particles with better contrast. In addition, radiation can cause damage to morphology, and shadowing the particles usually masks smaller aggregates. This case study shows that AUC is useful to characterise the aggregates formed by combining an organometallic hydrophobic part and a polymeric amphiphilic part, as DLS and TEM suffer from low resolution, thereby masking smaller particles in heterogenous solutions of self-assembled aggregates.

2.5.2 Circular dichroism spectroscopy (CD). CD spectroscopy is a form of light absorption spectroscopy that measures the difference in the absorbance of right- and left-circularly polarised light by a substance, which arise from structural asymmetry of the molecules observed.[91] CD spectroscopy has been widely used for assessing the secondary structure of proteins and performing studies on dynamic systems, such as the folding and binding of proteins.[92] There are few methods available to study supramolecular chirality; different microscopy techniques, such as SPM, SEM and TEM, allow the resolution of spatial images of the chirality in individual molecules or self-assembled supramolecular systems, but they typically require non-trivial sample preparation procedures. In contrast, optical characterisation techniques, such as CD, enable the chirality of particles to be resolved for supramolecular assemblies in solution, as well as to track the effect of external stimuli, such as metal ions, temperature, solvent, and pH on chirality.

Case study 5b. Parquette and co-workers, reported the impact of Cu^{2+} coordination on the assembly of 1,4,5,8-naphthalenetetracarboxylic acid diimide (NDI)-based amphiphiles (Fig. 9A).[93] The NDI-amphiphile contains lysine/Fmoc protected lysine headgroup on one end and metal-binding BIM ((indolyl)methane) unit on the other end of the molecular structure. TEM, DLS, SEM and AFM studies showed that **10** forms nanotubes at neutral pH and nonspecific aggregates at pH 2 in $CH_3CN:H_2O$ (1 : 1). A morphological change from nanotubes to vesicular structures was observed on addition of Cu^{2+} ions to **10** at pH 7 in $CH_3CN:H_2O$ (1 : 1). The effect of Cu^{2+} ions, solvents, and pH on the discrete self-assembled states of chiral **10** was studied using UV-Vis and CD spectroscopy.

The lysine containing amphiphile **11** forms nanotube assemblies at pH 2 but fails to bind to metals due to coordination of the free lysine headgroup. In contrast, **10** exhibits absorbance bands in the range of 240 nm (band II) and 358/378 nm (band I) corresponding to the NDI chromophore. These bands undergo red-shifting on changing the solvents from TFE (2,2,2-trifluoroethanol) to $CH_3CN:H_2O$ (1 : 1, pH 7), indicative of J-type aggregation. The CD spectrum showed cotton effects in the 300–350 nm and 350–400 nm ranges in $CH_3CN:H_2O$ (1 : 1) at pH 2 and 7, whereas there is no signal for the CD spectrum in TFE, indicative of a less efficient assembly process. The presence of an excitonic couplet at $\approx$240 nm, due to positive excitonic splitting of the NDI band II transition at pH 7, is indicative of P-type NDI helicity and formation of aggregated species. However, at pH 2, lower overall intensity of the CD bands and the smaller excitonic couplet at $\approx$240 nm suggested that the assembly process was inhibited, producing partial aggregates with opposite M-type NDI helicity (Fig. 9B). The binding of Cu^{2+} at pH 7 is monitored by UV-Vis and forms a 1 : 1 complex with an association constant of 2.07 $\times$ 10^4 M^{-1}. The binding and morphological change is further confirmed by a change in shape of the CD spectrum for **10** after the addition of Cu^{2+} ions.

The CD spectrum of **10**-Cu also shows cotton effects in the 300–400 nm range, but the shape of the transitions in the 225–275 nm and 320–400 nm regions were completely different when compared to **10** only. The excitonic couplet at 240 nm for **10**-Cu resembles negative chirality, with M-type NDI packing. These CD studies indicate different intermolecular monomer packing orientation of both **10**, and **10**-Cu (Fig. 9C). This case study demonstrates that CD spectroscopy provides a powerful tool to reveal the molecular packing in the chiral supramolecular aggregates.

Summary

The main advantages of AUC to study polymeric metallo-supramolecular assemblies involves the determination of absolute molar mass and d_H of aggregated species. A large range of molar masses can be analysed (from hundreds up to several million g mol^{-1}) using AUC in these weakly linked assemblies. Other methods, such as size exclusion chromatography or electrophoresis, are susceptible to errors caused by interactions with the matrix. In addition, mass spectrometry, though very accurate, does not normally preserve subunit interactions. CD

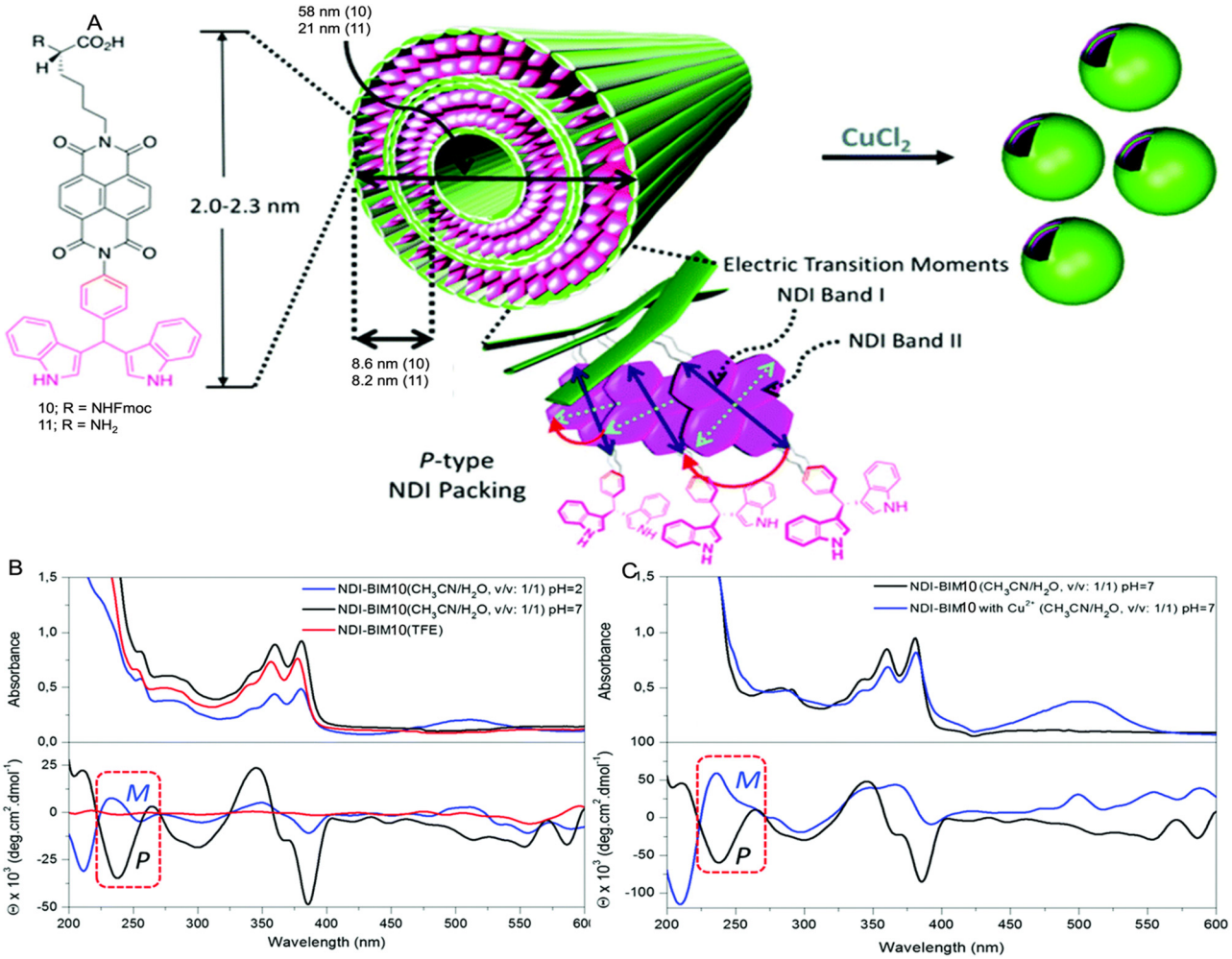

Fig. 9 (A) Self-assembly of NDI-BIMs **10** and **11**. (B) UV-Vis and CD spectra of 10 in $CH_3CN : H_2O$ (1 : 1) in pure TFE. (C) UV-Vis and CD spectra of 10 and 10-Cu in $CH_3CN : H_2O$ (1 : 1) at pH 7. Reproduced/adapted from ref. 93 with permission from RSC *Dalton Transactions*.

is an important spectroscopic technique which is used not only to study the chirality in self-assembled aggregates in solution, but also to monitor the dynamic behaviour of different structural states upon exposure to external stimuli, such as addition of metal ions, anions, temperature, pH, and solvents. Another powerful technique to resolve chirality is X-ray structural analysis, but this requires the formation of crystals. Amphiphilic systems typically do not crystallise therefore they are often not suitable for this methodology.

Limitations

A major disadvantage of AUC is the high cost of the device. Various methods such as Lamm equation fitting, van Holde–Weischet function and Gosting Fujita Lechner (GFL) principle are used to analyse these data. Each method is based on different algorithms and noise handling, and therefore can result in differences in data interpretation.[94] CD in chiral molecules is a relatively small effect (due to their small size relative to the wavelength) so does not provide atomic-level structural analysis. Therefore, CD is usually measured on macroscopic amounts of material in solution to get sufficient data. These ensemble-averaged measurements usually mask the sensitivity of CD to small structural variations between individual particles, or to the possible co-existence of opposite enantiomers in a system.

2.6 Critical aggregate concentration (CAC) determination

As previously described in the introduction, amphiphiles (including supramolecular amphiphiles) possess the ability to self-assemble into a variety of structures when in solution including, but not limited to, micelles, vesicles, nanotubes, bilayers, tubules, or reverse micelles.[1] At low concentrations, a dynamic equilibrium occurs where amphiphiles either aggregate into higher-order morphologies or adsorb at the surface interface of the solution, affecting the surface tension. Increasing amphiphile concentration increases adsorption until the surface is fully saturated and there is no longer an effect on surface tension. This concentration is defined as the CAC.[1,95] Once CAC is reached, any further increase in amphiphile concentration results in the continuous formation of the self-assembled morphologies in the bulk of the solution (Fig. 10). As the most documented morphology is the micelle, CAC is often referred to as CMC. However, depending on the chemical

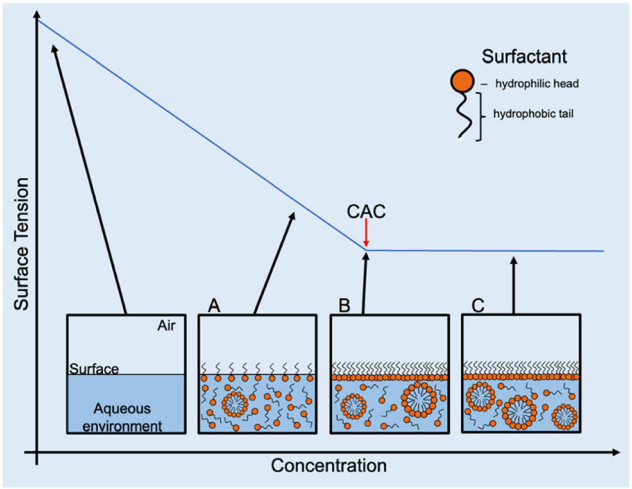

Fig. 10 Graphical depiction of CAC determination for amphiphilic species in an aqueous environment (including supramolecular amphiphiles): (A) amphiphiles adsorb at the surface in equilibrium with aggregate formation, (B) surface is fully saturated, and CAC is reached, and (C) continued aggregate formation as concentration of amphiphiles increases after CAC is reached.

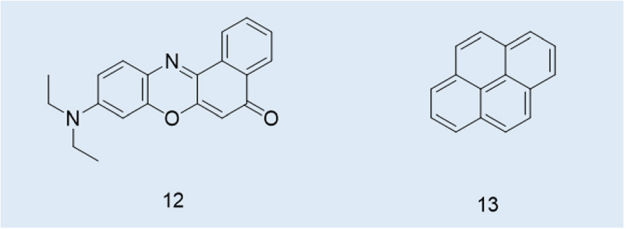

Fig. 11 Chemical structures of NR (**12**) and pyrene (**13**).

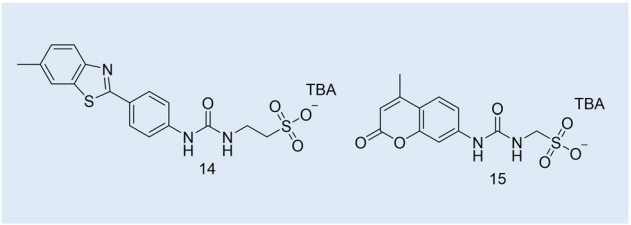

Fig. 12 Chemical structures of SSAs **14** and **15** used to develop the CAC OD-based microplate methodology. TBA = tetrabutylammonium.

structure of and the environment the amphiphile is in, the type of morphology formed can differ. For this reason, the term CAC is used instead, unless the exact morphologies present in solution can be ascertained.

2.6.1 Tensiometry. When CAC is reached, changes in molecular physical properties occur which can be observed by a variety of techniques. One of these properties is surface tension. To measure any changes in surface tension and obtain CAC, the Wilhelmy plate method can be used.[96,97] Here, a Wilhelmy plate is either immersed into or retracted from a solution. In both cases, surface tension exerts a downward force and pulls the plate into the liquid, and a surface tension reading can be obtained by measuring the force exerted on the plate. However, there are limitations of this method, including the need for a large number of samples and the risk of contamination of the Wilhelmy plate, affecting any measurements generated.

An alternative method to measure surface tension is the pendant drop method, which involves optically analysing the curvature or contour of a liquid drop and fitting the measured contour to one calculated using the Young–Laplace equation.[97,98] While this method is comparatively simple, requires less sample than others, and produces results that are easier to interpret, the main limitation is the lack of control over environmental temperature, which can affect CAC and thus distort any results obtained.[97,99]

2.6.2 Fluorescence spectroscopy. Fluorescence spectroscopy can be used to determine CAC by adding a fluorescent probe and measuring the uptake of the dye by the aggregates formed in solution and observing any changes in fluorescence emission.[100] Depending on the probe used, the change in fluorescence may increase or decrease. For example, the commonly used dye Nile red (NR; Fig. 11 and 12) only fluoresces in non-aqueous environments *i.e.*, upon increasing amphiphile concentration after CAC has been reached, the fluorescence intensity will increase as NR moves from the aqueous environment to the non-aqueous environment in the self-associated aggregate core. Alternatively, dyes that fluoresce in aqueous environments, such as pyrene (Fig. 11 and 13), produce a decrease in fluorescence intensity when under the same conditions.[16,101,102] However, using a dye may affect the structure, aggregation, or stability of the amphiphile system under analysis, or the dye itself may aggregate resulting in unreliable results, as previously reported.[102–104]

2.6.3 Optical density (OD). The limitations faced by using standard techniques to calculate CAC led to the development of an optical method using a microplate reader to obtain surface tension by monitoring variations in the surface curvature of

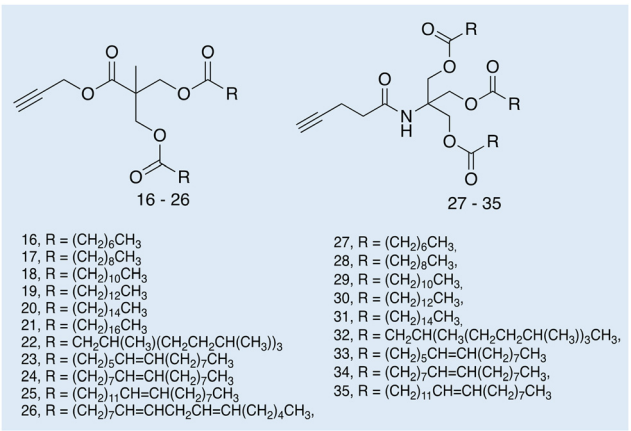

Fig. 13 Structures of amphiphiles **16–35** synthesised by Feast and co-workers. Reproduced/adapted from ref. 115 with permission from *Beilstein Journal of Organic Chemistry*.

aqueous translucent liquid samples.[105–107] Based on the Young equation, this alternative method relies on the meniscus of the sample acting as a lens to obtain the contact angle, θ, which then indicates the curvature of the meniscus *i.e.* when $\theta < 90°$, the meniscus is curved upwards; when $\theta = 90°$, the meniscus is flat; when $\theta > 90°$, the meniscus is curved downwards. By running optical density (OD) measurements with a vertical detecting light beam that passes through the surface of the sample, any variations in the curvature of the meniscus at the surface interface can be measured and, as the curvature of the meniscus is determined by the surface tension of the liquid, the surface tension, and thus CAC, can be calculated.[105,106] This method provides many advantages over standard, low-throughput techniques, allowing for controlled environments, automation, microlitres of sample, and simultaneous testing of multiple samples, making this a high-throughput process that eliminates the risk of manual error and contamination, lack of environmental control, the use of chemical probes, and overall time consumption. However, factors such as the material of microplates used and the use of solvents with a comparatively curved liquid surface (such as H_2O) reduce the sensitivity of the measurements and affect the data generated.

Case study 6a. Hiscock and co-workers built on existing OD-based methodologies and presented a new method to obtain the CAC of four SSAs (Fig. 3–5; Fig. 12, 14 and 15) over a range of temperatures.[108] After first estimating CAC using the pendant drop method at ≈291–298 K, Hiscock and co-workers then ran a series of OD microplate well scans at increasing concentrations and temperatures, and in triplicate to ensure the validity and reproducibility of any data obtained. It was found that CAC values calculated using the OD method were lower than those calculated using the pendant drop method, as shown in Table 3. However, it was hypothesised that the difference in CAC values may have arisen due to a second phase of self-association events, potentially enabling the definition of the three different phases of CAC determination as outlined in Fig. 11.

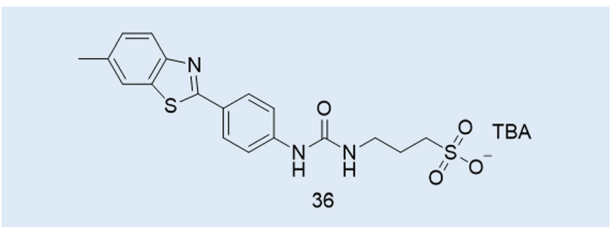

Fig. 14 Structure of a benzothiazole SSA, **36**.

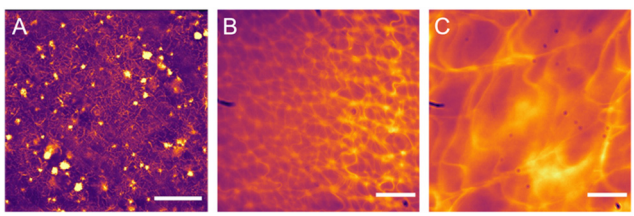

Fig. 15 Fluorescent microscopy images of self-associated fibres formed from (A) **4**, (B) **14** and (C) **36** (5 mg mL^{-1}) in and aqueous solution of Na_2SO_4 at 0.505 M. Scale bar A = 120 μm, B and C = 20 μm. Reproduced/adapted from ref. 5 with permission from RSC *Journal of Material Chemistry B*.

Table 3 Summary of CAC values calculated from OD microplate well scan and the pendant drop methodologies as reported by Hiscock and co-workers.[108] Adapted from ref. 108 with permission from RSC *Organic and Biomolecular Chemistry*

	CAC (mM)			
	OD microplate method			Pendant drop method
SSA	298 K	308 K	318 K	RT
4	0.41	0.46	0.48	0.50
5	8.91	8.69	7.99	9.54
14	1.51	1.49	1.37	1.92
15	14.86	19.64	14.42	16.20

Summary

This work demonstrates how determination of CAC is useful in understanding the self-associative abilities of supramolecular amphiphiles. This array of non-destructive, reliable, and accessible techniques allows the observation of properties directly linked to self-association events and CAC.

Limitations

Excluding OD, the techniques discussed within have many limitations including a lack of environmental control, contamination, requirement for a large quantity of samples, and the use of chemical probes. The use of microplates made of particular materials and/or solvents with curved surfaces reduce the sensitivity of OD measurements obtained.

2.7 Microscopy

Microscopy methods can either be destructive or non-destructive, and can be used to evaluate samples in varying states and environments.[109] The following subsections evaluate the use of these different microscopy methods for use in the characterisation of supramolecular amphiphile systems.

2.7.1 Atomic force microscopy (AFM). Conventional AFM is a technique used to obtain nanoscale high-resolution images of molecular assemblies, providing information relating to morphology, surface charge or surface impurities, leading to the determination of sample purity, size, and uniformity.[110–112] However, AFM can also be used in the solution-state (electrochemical-AFM), to discern the surface properties of any structure under analysis.[112] Within the amphiphile space, electrochemical-AFM has been used to observe the absorption of peptides at a hydrophilic silica/H_2O interface to allow the determination of CAC.[113]

2.7.2 Polarised light microscopy (PLM). Polarised light microscopy (PLM) uses polarising filters to assess the optical properties of a sample. In supramolecular chemistry, PLM is used to discern and understand the nanostructures of self-assembling materials and can be used to help characterise structures formed through amphiphile self-assembly. PLM has been used in this way to characterise differences between

systems containing a range of gemini-type zwitterionic amphiphiles, such as those shown in Fig. 13. This is an example subset of molecules from the original 80 amphiphile library synthesised by Feast and co-workers, containing variations in saturation, head-group geometry, and alkyl chain length. Here the lyotropic phase behaviour for this class of supramolecular amphiphile was determined using cross-polarised light microscopy.[114,115]

This was achieved by elucidating the thermotropic liquid-crystalline (LC) behaviour towards the development of specific LC phases. The LC phases were observed through PLM with the images showing the differences in structure across samples of varying functional group composition. This work aims to highlight the importance of the spatial arrangements of functional chemical groups when designing amphiphiles with novel uses and applications.

2.7.3 Fluorescence microscopy. Fluorescence microscopy is an optical microscopy technique that uses principles of fluorescence to observe the morphology of sample materials. This fluorescence can be intrinsic to the molecule itself or can be provided through the addition of fluorescent dyes, tags, or labels.[116] For supramolecular amphiphile systems, this enables the direct visualisation of any resultant self-assembled structure directly within the solution-state.

Case Study 7a. Here we highlight the potential use of this technique for the characterisation of supramolecular amphiphile systems, through the following work of Hiscock and co-workers, specifically relating to intrinsically fluorescent SSAs such as **4**, **14** and **36** (Fig. 3 and 4; Fig. 12 and 14; Fig. 14, **36**). The only difference between these structures being the length of the alkyl spacer between the urea and sulfonate functionalities (**4** = methyl, **14** = ethyl, **36** = propyl).[5]

Due to the intrinsic fluorescence properties of **4**, resulting from the incorporation of the benzothiazole moiety within the anionic component of this amphiphilic salt, systems incorporating **4** were studied through the use of fluorescence spectroscopy.[117] Here noticeable changes in excitation and emission properties were observed as the self-assembled structures present altered upon changes in temperature. Due to the intrinsic fluorescence properties demonstrated by this subclass of benzothiazole incorporated SSA, fluorescence microscopy was not only used to provide insight into the mode of therapeutic action for this class of compounds, but also to study changes in the morphology of those self-assembled structures produced in different solvent environments.[2,37,117] For example, members from this benzothiazole appended sub-class of SSAs have been shown to morph from spherical aggregate to gel fibre under aqueous conditions, upon the addition of salt and a subsequent annealing process, enabling real-time observation of those structures formed.[111] In addition, and as highlighted in Fig. 15, this also enabled SSA – self-associated structure property analysis. Here the changes in the morphology of those fibres formed, through a stepwise change in SSA (the addition of one CH_2) could clearly be observed without the removal of solvent.[5]

2.7.4 Transmission electron microscopy (TEM). TEM uses a beam of electrons to discern the atomic arrangements of localised areas of material. The ability of TEM to form images of the microstructure and structural variations between regions provides a vital role for this technique to enable the informed design and characterisation of amphiphilic materials.[118] Ludlow and co-workers used TEM to characterise the morphology and self-assembly of a series of long-chain amphiphilic metallotriangles, as shown in Fig. 16.[119]

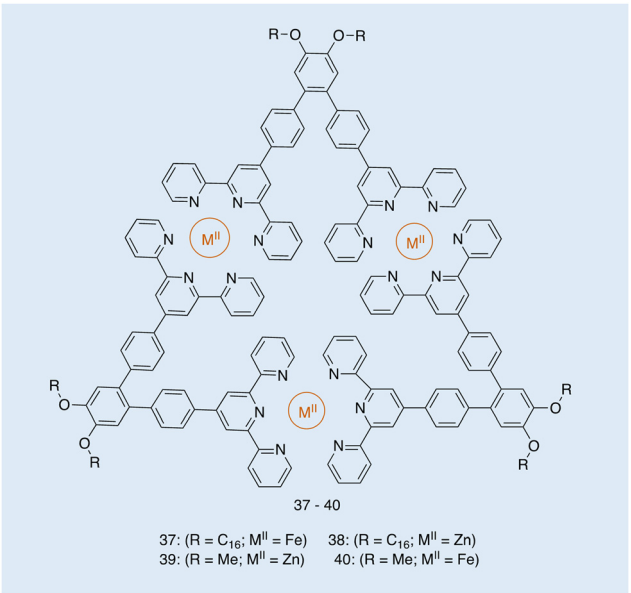

Fig. 16 Structure of metallotriangles **37–40**, synthesised by Ludlow and co-workers. Reproduced/adapted from ref. 119 with permission from Taylor and Francis *Supramolecular Chemistry*.

From the images obtained, the authors of this work were able to evaluate the extent to which the metal type and the R groups of varying amphiphilicity affected the morphology of these metallotriangles. TEM shows the structural differences to be dependent on the amphiphilic nature of the molecule and the self-assembly around metals of different lability.[119]

2.7.5 Scanning electron microscopy (SEM). SEM produces detailed images of surface topology, crystalline structure, and chemical composition of a material through scanning a beam of electrons across the material's surface.[120] SEM has been used to show the self-assembled structures of supramolecular amphiphilic gel fibres.[121–123] SEM exhibits a large depth of field, which is incredibly beneficial as it allows observation of a larger area of sample including larger self-assembled structures.[124]

The biggest disadvantage of SEM is that this technique only allows for observation of the surface of a molecule. This can be overcome by employing the technique of focused ion beam-SEM (FIB-SEM). The FIB removes the surface layer of the structure before another image is taken. This process is continuously repeated until a 3D image is formed.[125]

Case study 7b. Cano and co-workers have synthesised a series of molecules containing polar lactic acid head groups and lauric acid tails joined through a linker, Fig. 17.[123] These molecules have hydrogen bond-directing groups that support molecular self-assembly, resulting in the formation of flexible fibres, that when entangled, form a 3D network, resulting in the

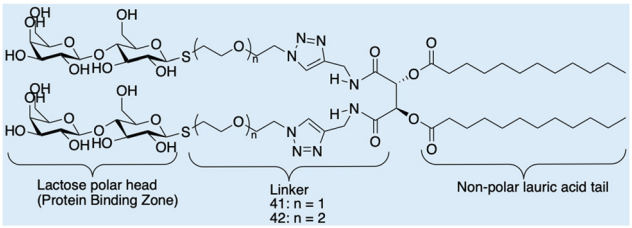

Fig. 17 Chemical structures of lactose and lauric acid-based **41** and **42**, observed by Cano and co-workers through SEM and E-SEM. Reproduced/adapted from ref. 123 with permission from RSC *New Journal Of Chemistry*.

production of a material which demonstrates viscoelastic properties. Cano and co-workers analysed the morphology of the hydrogels formed using SEM and environmental-SEM. The data obtained show entangled nanofibers that form a dense 3D network. The morphologies of these networks produced through the self-assembly of **41** and **42**, were analysed and show fibrils produced from **41** are larger than those produced from **42**, attributed to the aggregation of the assemblies caused by solvent evaporation.

2.7.6 Other electron microscopy techniques. Cryo-electron microscopy (Cryo-EM) is a technique rapidly growing in use and availability. Here, samples are cooled to cryogenic temperatures through plunge freezing before being imaged using a form of EM.[126] Cryo-EM techniques can be further sub-divided into two different categories, single-particle-cryo-EM (SPA cryo-EM) and cryo-electron tomography (cryo-ET).[127] Through the use of cryo-EM, structures and samples can be imaged in their closest natural state, making this technology extremely promising for the observation of amphiphiles in a near *in situ* state.[128]

In SPA cryo-EM, a single 3D reconstruction is obtained by combining TEM images of the sample in different orientations. This reconstruction is normally the result of thousands of separate TEM images and 2D projections that are then reconstructed into a 3D image through Fourier inversion.[127] Since its development, SPA cryo-EM has been used extensively to observe assembled amphiphiles, most commonly proteins, in a near *in situ* state.[128–131] However in contrast, cryo-ET uses a series of images taken at different tilt angles that when combined computationally produce a 3D sample image.[126] Cryo-ET with nanometre detail has been used to visualise the complex aggregation of amphiphilic copolymers.[132]

Summary

Similar to other methods presented in this review, each microscopy technique commonly used for the characterisation of supramolecular amphiphiles has different advantages and disadvantages, most notably different structural observations in different physical states. As such, these techniques are best used in tandem to give a full picture of any self-assembled structures present.

Limitations

AFM: Destructive technique.

PLM: Lower resolution, surface technique.

Fluorescence microscopy: Relies on the use of fluorescent tags or fluorophores within the molecule.

TEM: Destructive technique and problems of radiation damage to sample.

SEM: Disadvantages: surface structure only, 2D images and risk of radiation damage to sample.

Cryo-EM: Cannot be used for thermo-reversible samples and is a highly costly, lengthy process with lower availability compared to other microscopy techniques.

2.8 Working with supramolecular amphiphiles in a biological setting

Supramolecular amphiphiles are gaining interest for translation into a clinical setting. For example, SSAs have been shown to exhibit a ''druggable'' profile,[3] improve the efficacy of existing drugs including anticancer agents[2,3] and antimicrobials.[3] Amphiphilic systems are ideal candidates for development as drug delivery systems, acting as carriers for poorly soluble therapeutic agents, in addition to offering modified release profiles for encapsulated molecules.[4] However, the desired characteristics for lead candidates in drug development[133] also apply to supramolecular amphiphiles. Prior to the commencement of *in vitro* (with cells outside a living organism) or *in vivo* (within a living organism) work, key factors include determining the purity, stability, and solubility of the amphiphile in question. Amphiphile purity is necessary to accurately determine if any biological activity/unwanted effects are unambiguously because of the amphiphile,[133] with a desired purity $\geq$95% for biological testing.[134] Supramolecular amphiphiles for use in a biomedical application must be water soluble, as otherwise they are incompatible with any biological system.[135,136] There are structural components that can increase the water solubility of an amphiphile, such as inclusion of a carbohydrate,[137] use of bola amphiphiles,[1] and the addition of polyethylene glycol to the amphiphile system.[138]

In addition, amphiphile monomers or aggregates that interact with components of biological fluid will influence the supramolecular and covalent stabilities, and thus functionality of the amphiphile.[4] Stability should be assessed in simulated *in vivo* medias (*e.g.* mock serum, simulated intestinal fluid) and results used to guide structural modification, diagnose poor oral bioavailability, prioritize chemical series, and evaluate formulations for improving stability.[139] Stability strategies have been discussed by Lu and co-workers,[140] and stability assessments in biological media have been discussed by Feiner-Gracia and co-workers,[4] with other key introductory texts referenced here.[133,134,141]

2.8.1 Physiological considerations for design of amphiphiles as drugs. Using biological factors as cues for rationally designed characteristics of a supramolecular amphiphile can facilitate a targeted ''smart'' drug design. Self-assembly is an equilibrium process whereby aggregates form when the concentration of molecules exceeds CAC, as described in Section 6.[142,143] Due to the chemical complexity of an *in vivo* environment, supramolecular amphiphiles with a high CAC, may dissociate when administered intravenously (i.v.) upon dilution in the plasma.[4,140] CAC is often calculated in H_2O or phosphate buffered saline, which does not reflect the composition of

serum.[4] Aggregates may undergo several further environmental changes, as well as contact with numerous proteins, salts, lipids, and cells; this could result in a carrier molecule prematurely releasing encapsulated therapeutic content, consequent side effects, and/or decrease in efficacy.[140]

Other *in vivo* physiological factors that will influence aggregates include pH (optimum pH 7.4),[144] temperature, salinity of blood/tissue fluid,[117] shear flow of blood,[145,146] and light (UV is commonly used but toxic to living cells).[135,147]

Physical factors of the aggregate that can influence the pharmacokinetics of supramolecular amphiphiles include the size and shape of the aggregate, charge distribution, the lipid solubility, and the extent of water-solubility, as these will influence circulation time and transport *in vivo*.[148] An optimal supramolecular structure would possess an elongated shape with a size range of 12–50 nm and be neutral/not charged to achieve optimum vascular and interstitial transport and cellular uptake.[148] Lipinski's 'rule of 5' also present structural characteristics that will affect the pharmacokinetic/dynamic profile.[149]

Case study 8a. As described, there are several *in vivo* characteristics that will interfere with amphiphiles, however, these parameters offer potential tunability to amphiphile activity. Cancer cells have a lower mitochondrial membrane potential than normal cells (−180−−220 and −120−−160 mV respectively)[150] and dysfunctional mitochondria with a disrupted proton gradient and a more negatively charged membrane.[151] Jeena and co-workers sought to design a positively charged lipophilic peptide amphiphile L-Mito-FFY (**43** Fig. 18A) that would preferentially accumulate in the mitochondrial matrix of cancer cells, due to the addition of the delocalised lipophilic cation triphenylphosphonium (TPP), and self-assemble into a fibrous structure inside the mitochondria.[152] This would both address the issue of undesirable activity at

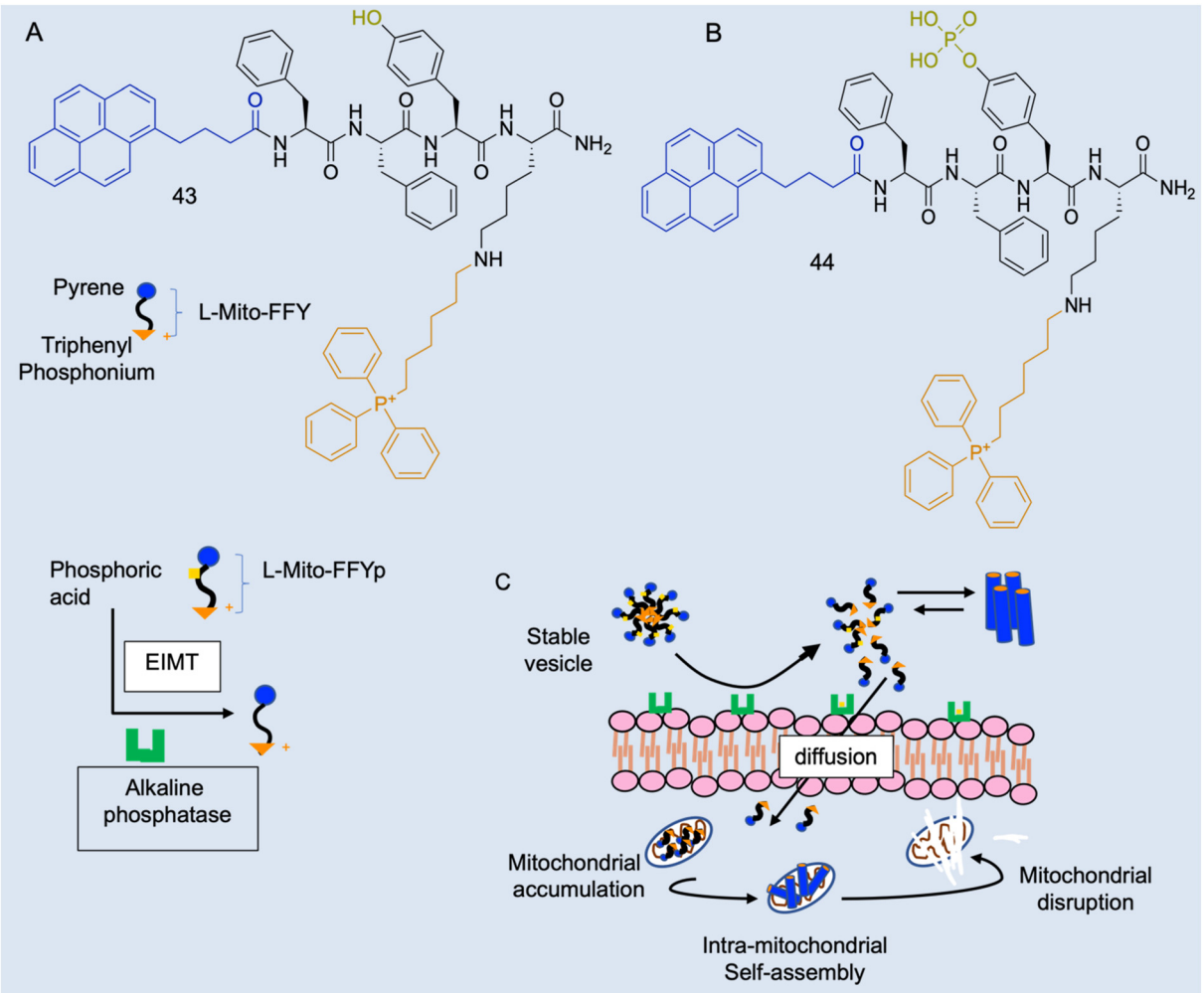

Fig. 18 Schematic illustration of the enzyme-instructed morphology transformation (EIMT) of an ALP-responsive micelle. (A) Chemical structure L-Mito-FFY **43**. (B) Chemical structure of L-Mito-FFYp **44** and schematic showing EIMT of **44** by alkaline phosphatase into **43**. (C) Schematic showing *in vivo* alkaline phosphatase enzyme on osteosarcoma cell surface induces the transformation of **44** micelles to positively charged **43**, which are attracted to the highly negative mitochondrial membrane and enter the cell *via* free diffusion to target the mitochondria *via* the TPP moiety. Inside the mitochondria, **43** passes the CAC and self-assembles into nanofibers to induce mitochondrial dysfunction leading to cell death. Reproduced/adapted with permission from *RSC Chemical Biology*.[154]

healthy cells, as well as overcome potential problems with aggregate stability in the plasma.[4] *In vitro* work found **44** had a 10-fold greater accumulation in cancerous cell mitochondria than healthy cell lines, causing significantly more mitochondrial dysfunction in these diseased cells.[153,154]

The subsequent *in vivo* work found that, whilst **43** was not as efficacious as *in vitro*, combination therapy of **43** with fluorouracil significantly reduced gastric tumour volume and increased apoptosis, more than monotherapy, resulting in these agents synergistically enhancing reactive oxygen species.[153] However, a positive molecule has potential undesirable interactions with negatively charged serum molecules and serum proteins *in vivo*. Osteosarcoma cells overexpress alkaline phosphatase (ALP), so **43** was developed into L-Mito-FFYp (Fig. 18B, **44**), which forms physiologically stable micelles with a negatively charged surface and carries ALP substrate phosphoric acid.[154] When in proximity to the ALP-overexpressing cells or osteosarcoma cancer cells, these micelles disassemble in response to the excessive ALP becoming the positively charged **43** peptide monomer, and subsequently diffuse through negatively charged cell membranes and self-assemble as shown in Fig. 18C.

Summary

Supramolecular amphiphiles enable targeted ''smart'' drug design. However, any resultant aggregated structures produced must still exhibit a desirable selectivity profile, permeability, stability, and biological potency in order to be considered ''druggable'' agents. Consequently, this case study illustrates how to work with and adapt supramolecular amphiphiles in a biological setting to achieve this.

Limitations

The unique behavior of supramolecular amphiphiles offers promising avenues for targeted drug design and novel therapeutics, but there are limitations to consider. If CAC is high, upon dilution in the blood, aggregates can release their drug cargo early,[155] however, low CAC may also correlate with toxicity of the amphiphile.[156] Aggregates can have limited loading capacity (<5% w/w) with pharmaceutically acceptable excipients limiting potential use as drug delivery systems.[157] Whilst supramolecular amphiphiles offer the means for targeted drug design, these systems are not broadly applicable across multiple diseases, and it is difficult to predict and control the molecular assembly dictated.[158] Unless multi-component amphiphile systems are used, the structures they form are homotypic and thus have limited functional complexity and tunability once aggregated.[159]

2.9 Free online *in silico* tools for molecular physicochemical and ADME predictions

Drug discovery and material scientists use *in silico* (experimentation conducted by computer modelling or simulation) programs to predict the physicochemical and ADME (absorption, distribution, metabolism, and excretion) properties of molecular targets, to influence design and enhance properties relevant for specific applications, thus reducing synthetic liabilities, and improving safety profiles. This is particularly important for those with limited physical resources.[160]

Free online *in silico* physicochemical and ADME prediction tools are valuable resources for drug design and material development, for several reasons: cost-effective – no need for expensive software; accessible to a wide range of researchers with a user-friendly interface and no need for pharmacokinetic expertise; rapid screening – efficient evaluation of multiple compounds, saving time; predictive accuracy – these established computational models and databases use experimental data validation – aiding selection of drug and material candidates; and *in silico* optimisation – this allows for prediction of potential issues of drugs and materials at various stages of development and earlier improvement. However, there are limitations to this technique: confidentiality of data is not guaranteed; no servers will cover all the parameters you need; calculation methods can change – this will need to be evaluated with usage; and variability between free tools due to differences in algorithms, models, or data sources and limited data on the applicability of certain types of amphiphiles. Due to these limitations, the use of these tools should only aid investigations into the viability and development of a potential drug or material, whilst supporting the experimental evaluation.

Several comprehensive reviews have been published, detailing free online pharmacochemical and ADME servers, as well as directory links for those tools and databases.[161–165] The free software programs predict a variety of properties: $\log S$ (aqueous solubility), $\log P$ (octanol–water coefficient), $\log D$ (octanol–water distribution coefficient), TPSA (total polar surface area), HIA (human intestinal absorption), Caco-2 (human colon adenocarcinoma cell line; to understand the permeation of membranes), PPB (plasma protein binding), BBB (blood brain barrier penetration), V_d (volume of distribution; the ability of a drug to diffuse to several tissues from the blood flow), metabolism, CL (clearance), toxicity, P-gP (*P*-glycoprotein) and pK_a (acidity coefficient). Currently, there are three ADME software programs that include drug-likeness data: SwissADME,[166] ADMETlab[167]/ADMETlab2.0,[168] and FAF-Drugs4[169] using *e.g.*, Lipinski, Veber, Egan, Ghose, Muegge, Oprea, Varma, GSK's 4/400, and Pfizer's 3/75 rules.[161–165]

Case study 9a. Scognamiglio and co-workers illustrated the self-assembly of the thyminyl L-tryptophanamide (TrpT) construct (Fig. 19A) into supramolecular networks and detailed its potential as a drug delivery nanosystem.[170] The nanoaggregates formed in aqueous solution (Fig. 19B and C), are characterised using some techniques discussed in this tutorial review: DLS, CD, fluorescence or UV-Vis spectroscopic measurements, and SEM.

The researchers demonstrated that the TrpT nanostructure encapsulated the physicochemical suboptimal curcumin (Fig. 19D).

Inputting the structure of TrpT into the SwissADME server, generated a unique simplified molecular input line entry system (SMILES), which is a fingerprint code for a particular chemical structure. The SMILES string enabled the predicted physicochemical and ADME data of **45** – Fig. 20 is the SwissADME pictorial layout of the predicted data.

The authors hypothesised that the Trp-T-curcumin adduct increased the polarity of curcumin to become more drug-like, supported by the idea that the optimum drug-like range for good

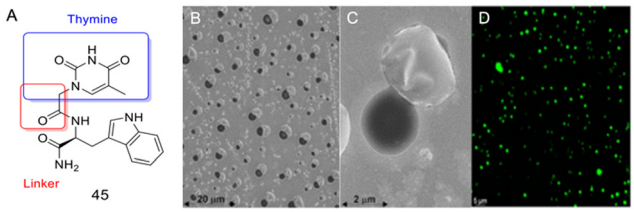

Fig. 19 (A) TrpT, **45**. (B) and (C) Morphology of TrpT self-assembly in aqueous media (SEM analysis). D) Curcumin encapsulated (green) by TrpT nanovesicles (confocal microscopy analysis). Reproduced/adapted from ref. 170 with the permission of Creative Comms Attribution 4.0 International License (https://creativecommons.org/licenses/by/4.0/).

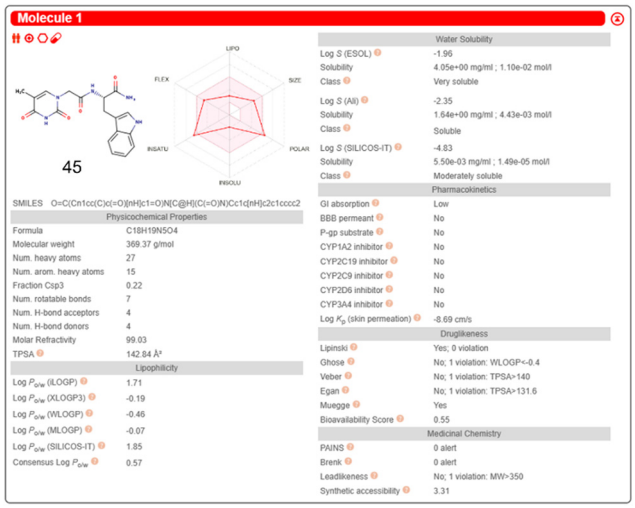

Fig. 20 SwissADME free online server generation of physicochemical and ADME properties of **45**. This diagram illustrates an example presentation of the SwissADME data layout after input of a molecular structure or SMILES string. Reproduced/adapted from ref. 166 with the permission of Creative Comms Attribution 4.0 International License (https://creativecommons.org/licenses/by/4.0/).

cell permeability is $0 < \log P < 3$. The predicted ADMETlab $\log P$ of free curcumin is 3.4, while the predicted ADMETlab $\log P$ of the Trp-T-curcumin adduct is 3.1, potentially making the Trp-T-curcumin adduct more bioavailable than the free curcumin.

Case study 9b. Hiscock and co-workers determined the druggable potential of selective antimicrobial SSAs through *in vitro* and *in vivo* DMPK (drug, metabolism, and pharmacokinetic) studies.[3] Based on the experimental DMPK data, SSA **5** (Fig. 3 and Fig. 21A) was determined as the lead compound suitable for further therapeutic drug development.

To validate the comparative accuracy of different parameters of the *in silico* data *versus* the *in vivo* data, and for the purpose of this review, the SwissADME SMILES string for **5** is shown in Fig. 21C, and this enabled the generation of the ADMETlab 2.0, $\log D$, PPB, $t_{1/2}$, and V_d data. The results show that, whilst *in vivo* $\log D$ *versus* ADMETlab 2.0 $\log D$ is different, *in silico* PPB, $t_{1/2}$ and V_d are a good indication of how SSA **5** behaved *in vivo*.

Both case studies highlight the limitations of using SMILES to generate physicochemical and ADME data using the free

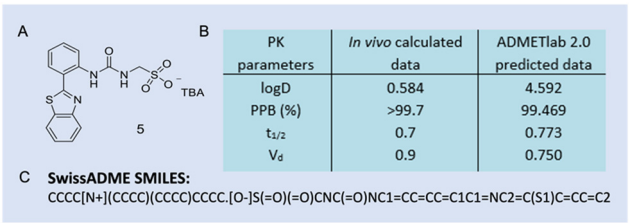

PK parameters	*In vivo* calculated data	ADMETlab 2.0 predicted data
logD	0.584	4.592
PPB (%)	>99.7	99.469
$t_{1/2}$	0.7	0.773
V_d	0.9	0.750

Fig. 21 (A) The structure of **5**, TBA = tetrabutylammonium. B) Table of *in vivo* data (mouse blood PK studies, n = 3, intravenous route, and dose of 1 mg kg^{-1}) *versus in silico* generated data for **5**. $\log D$ = $\log P$ at physiological pH, PPB (%), $t_{1/2}$ (h) = elimination half-life = the time required for plasma concentration of a drug to decrease by 50%, and V_d (L kg^{-1}) = apparent volume of distribution = total amount of drug in the body/drug concentration in plasma. ^{3}C) SwissADME SMILES string of **5** and is reproduced from ref. 166 with the permission of Creative Comms Attribution 4.0 International License (https://creativecommons.org/licenses/by/4.0/).

software. The use of SMILES strings does not consider the non-covalent interactions of these supramolecular amphiphiles, therefore, researchers potentially need to use the closest predicted structures using covalent bonds to support hypotheses.

Encouragingly, steps are in progress to overcome these SMILES limitations for the *in silico* prediction of supramolecular drug-like compounds. Recently, Olsen and co-workers published BigSMILES, an annotation method that is an extension of, and compatible with SMILES, which shows potential to understand non-covalent bonds in supramolecular assemblies.[171] Each type of interaction in supramolecular assemblies have their own annotation (Fig. 22); this has the capability to add non-covalent bonds to even smaller molecules than exemplified within this work. Additionally, this software has the potential for use in other computational programs to determine physicochemical and ADME properties of supramolecular molecules, including supramolecular amphiphiles.

Summary

SwissADME and ADMETlabs are useful *in silico* tools that generate physicochemical and ADME predictions for

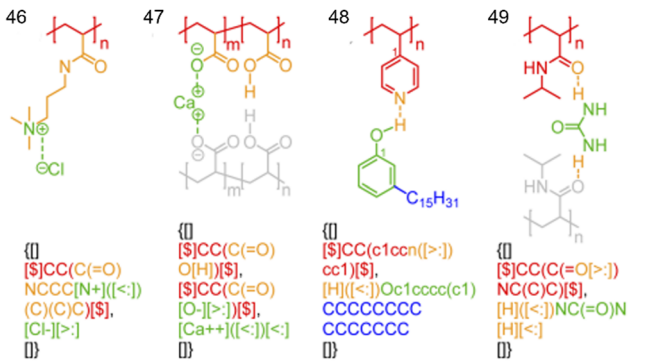

Fig. 22 Chemical structures of **46–49** showing non-covalent bond annotation in typical polyelectrolytes and hydrogen bonding polymers. The colours of the bonds and atoms in the diagram correspond to the identical colour of the BigSMILES string (faded grey components not included). Reproduced/adapted from ref. 171 with the permission of the RSC *Chemical Science*.

supramolecular amphiphiles. They are accessible, cost-effective and enable rapid screening of multiple molecules in a time efficient manner. This allows for some predictive accuracy and *in silico* optimisation of lead compounds to help mitigate problems arising in development of molecular targets.

Limitations

There is a variation between parameters for free online physicochemical and ADME predictive tools, and calculation methods may change over time for each program. There is variability between each program, in terms of how the data is generated, and confidentiality of data is not always guaranteed. The biggest limitation for supramolecular amphiphiles is that current online *in silico* predictions are not capable of incorporating non-covalent interactions in their calculations. Free online *in silico* generated data should be used cautiously to aid molecular design, and in conjunction with experimental data to help optimise drug-like or material leads.

2.10 Quantitative structural activity relationship (QSAR) and other computational techniques

QSAR methods are a growing and developing field that was initiated in the 1960s,[172] and are used to predict a target property using structural chemical features,[173] such as SwissADME descriptors. The model adjusts the weighting of the features to accurately predict the target values from the dataset. The models are trained on a high percentage (often $\approx$ 80%) of the data, known as the training set, here the model fits to the data and the model's weights are set. To validate the model's accuracy, a small subset of the data ($\approx$20%) is withheld when the model is trained. The model takes in the features of this unseen subset of data and scores the model for accuracy based on the differences between the predicted and the actual target values.

QSAR methods are only as good as the data they are trained on; the datasets used within many computational predictive studies for amphiphilic compounds. For example, CAC has been shown as a relevant property for MIC (minimum inhibitory concentrations (MIC) is defined as the lowest concentration of an antimicrobial that will inhibit the visible *in vitro* growth of a bacteria when compared to a control) prediction *via* computational method models and the obvious relevance to real-world applications in drug discovery.[34] CAC predictions are usually small ($<$100 molecules) to ensure data can be validated. These datasets often focus on subsets of amphiphiles with similar structures.[34,174,175] Features are specifically chosen to model each type of amphiphile resulting in QSAR models that are specific to the subset of amphiphiles the model is trained on.

Features for the QSAR models can either be generated computationally, or experimentally derived. Experimentally derived descriptors are less widely used in modelling due to the time taken to synthesise the molecule, run physicochemical experiments, and grow bacteria or cells (if the experiment is an assay). This makes these descriptors – which in some cases are the target of the model – very condition/run dependent with high experimental error. On the other hand, computationally derived descriptors have the advantage of being easily generated from widely available software libraries and packages such as RDKit[176] or SwissADME.[166] This allows the models to be used to predict the desired properties before the lead molecules are synthesised, aiding in the decision process, as shown in Fig. 23. The molecular representations are generated from the SMILES containing information about molecule connectivity, charge, and atom coordinates/properties. From this file, an image of the molecule can be generated, and molecular descriptors are calculated.

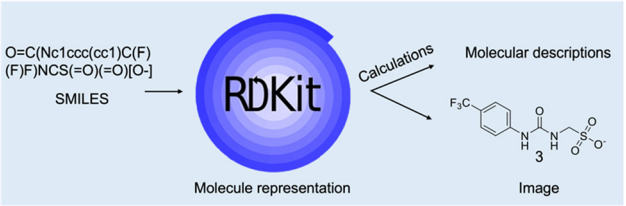

Fig. 23 The generation of molecular descriptors from a SMILES string using the RDKit library.[176] The figure depicts the anionic group from **3**.

Multi-linear regression (MLR) is the most widely applied QSAR model throughout literature for modelling CAC values due to its simplicity and effectiveness on small datasets.[172,174,175] This model works by finding coefficients-feature pairs that best predict the target data which, in this case, is CAC. This is shown in eqn (1), where Y is the target data for the model to predict, X_1 to X_n are the features used in the model, β_1 to β_n are the coefficients associated with each feature, and β_0 is the correction factor.

$$Y = \beta_0 + \beta_1 X_1 + \beta_2 X_2 + \ldots + \beta_n X_n \quad (1)$$

Another popular model is an artificial neural network (ANN), a multilayer perceptron (MLP) is a form of ANN with multiple hidden layers, an input and an output layer as shown in Fig. 24. For prediction each neuron in the input layer receives data, in QSAR modelling these are often molecular features on a molecule, weights and biases are applied to the data and passes it to the first layer of neurons in the hidden layer where an activation function can be applied. Weights and biases are applied to the output from the first layer of neurons in the hidden layer and this is passed to the next layer of neurons where again where an activation function can be applied.

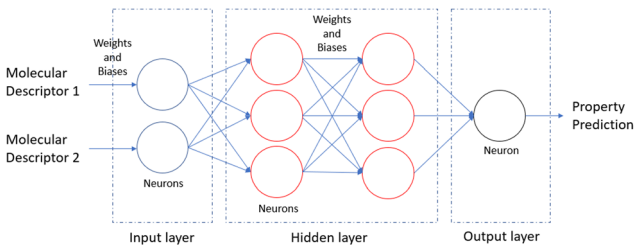

Fig. 24 General format of an MLP-ANN and how it can be applied to QSAR modelling. The example above has one input layer, two hidden layers comprising of three neurons each, and an output layer with a single neuron. The model takes in molecular descriptors and outputs a prediction of a physical property of a molecule (such as CAC).

Finally, the output from the hidden layers of neurons is passed to the output layer and the prediction is made.

ANN-MLPs can perform complex mathematical transformations on data using layered combinations of weights and biases. When this is used in combination with activation functions at each neuron, gives ANN-MLPs the ability to pick up non-linear trends within data. Despite their advantages, ANN-MLPs can be a difficult type of model to apply to QSAR modelling due to limitations in the size of the datasets available, as these models are data greedy.

Case study 10a. Rahal and co-workers applied three models: MLR, partial least square, and MLP-ANN, to a small dataset of 50 anionic surfactants, which have diversity in counter cation and anionic groups, variation in branching, and length of hydrophobic chain.[172] This dataset was taken from three sources within literature, and all were recorded as being measured at 25 °C in purified H_2O only. Finally $-\log_{10}$CAC was calculated to a normalised data spread and constant error over the entire data range.

The authors calculated 11 145 computational descriptors from the SMILES and from these, seven descriptors were selected. Several models were trained using 2 to 7 of these descriptors and statistical parameters were used to compare the accuracy of the model as the number of features was increased from 2 to 7. Four descriptors was the point at which adding additional descriptors no longer significantly improved the model's prediction. The selected descriptors were ATSC7v, ATSC5e, nAtomLAC and ETA_Epsilon_3 which, though calculated based on the structure of the molecule, are not as explainable as descriptors shown in case study 10b. The data they used fits within their chemical applicability domain- the structures and mechanisms of action that the QSAR models can reliably predict- of anionic surfactants and outlines the risks of extrapolating beyond the data used to train the model.

The authors evaluated modelling from six other research papers highlighting only one of these examples included a test set for external validation of the models. This may be due to the small dataset sizes used for these projects where the selection of the test/training subsets can impact model performance. However, a lack of external validation can lead to overfitting of the models not being picked up, making them potentially not generalisable even within their applicability domain. It was concluded that the descriptors used for the model encompassed information about the hydrophobic chain length and electronegativity of the molecules, which were linked to the process of micelle formation. Of the three models, the MLP-ANN was concluded to be the most effective with the highest-scoring statistical parameters.

Case study 10b. It is important to note that physical properties of supramolecular amphiphiles can also be predicted using molecular dynamics (MD) simulations and density functional theory,[177] however, when compared to small QSAR models, these methods are expensive in computational cost. Unlike traditional predictive models, MD does not rely on well-curated, validated and understood datasets.

The two methods can be used together as shown by Van Lommel and co-workers.[178] MD simulations were used to generate four descriptors to encapsulate information about the nanostructure: hydrogen bonding percentage (HB%), relative end-to-end distance, and relative solvent accessible surface area (rSASA). HB% is defined as the percentage of donor and acceptor atoms with a distance between them of <3 Å averaged over the course of the simulation. These descriptors have direct chemical relevance, making models trained using them more interpretable.

Simulation time frames of 1 μs were tested to calculate the rSASA descriptor. The error on the average rSASA value across all time steps after 50 ns had an error of 13% when compared to the true value after 1 μs. Therefore, the simulation time used to generate all descriptors chosen by the authors was 50 ns as a trade-off between the accuracy of the generated descriptor, and computational resources.

The researchers used these descriptors to train QSAR models including an ANN and a decision tree model (that predicts its target using a flowchart-like algorithm) to predict whether a molecule would dissolve, precipitate, or form a gel in six different solvents on a dataset of 11 molecules, 1 test and 10 training. These models outperformed those using random descriptors, and the ANN had entropy $R^2 = 0.82$ for the training set and $R^2 = 0.93$ for the test set (where an ideal $R^2 = 1$).

2.10.1 Data set size limitations and implementation of larger datasets. Larger datasets for both CAC and MIC are available within the literature, though these are difficult to curate. The National Standard Reference Data Series have a curated dataset of CAC values from literature between 1922–1962 containing 5000 entries for 721 surfactants/amphiphiles ranging across different domains.[179] The dataset is well curated with an accompanying paper that categorises each experiment in terms of material purity and methods precision/accuracy. However, being an older piece of research, these data are still held in pdf format and therefore not machine-accessible. A more modern example of a larger dataset is the Shared Platform for Antibiotic Research, a large, curated dataset of biological assays for a wide variety of molecules.[180] These data are available as spreadsheets, and have been both automatically gathered from the literature and then curated by experts. If these data were to be carefully curated, it may be possible to train a more reliable QSAR, however, there may not be enough supramolecular molecules to make QSAR modelling relevant to the supramolecular applicability domain.

Summary

Applying QSAR methods to predict the properties of supramolecular amphiphiles is a growing and promising field. QSAR methods have the capability to predict properties before molecules are synthesised, and thus aid in the understanding of how to modify molecules to enhance specific properties. Using traditional QSAR modelling in conjunction with MD-generated descriptors allows the QSAR models to be trained on descriptors generated on the larger nanostructures of supramolecular amphiphiles, which increases the amount of information provided to the models for the supramolecular applicability domain as well as making the models more explainable.

Limitations

Caution must be taken in understanding the generalisability of models and accurately evaluating their performance and limitations, as well as the selection of models themselves. It is computationally expensive to generate descriptors using MD directly relevant to larger nanostructures. Models trained are often only effective within their applicability domain. The real limitation of QSAR modelling is data access and validity, due to the lack of consistency of assay/experimental data across groups due to experiments being carried out for different purposes. A large, curated repository of supramolecular experiments and data could allow for significant gains in understanding the physical properties and mechanisms behind the activity of supramolecular amphiphiles.

3. Conclusions

This review emphasises that within the field of supramolecular chemistry, there is no common standard or single tool for the comprehensive characterisation of supramolecular amphiphiles. When faced with this challenge, Hiscock and co-workers developed an effective multicomponent experimental approach for characterising these complex systems as outlined in Fig. 24.[11,15,34,36,37,41,47,48,181,182] This extensive systematic approach combines multiple complimentary characterisation techniques in the solution- and solid-state, as well as in the gas-phase. Using this approach enables a comprehensive data set to be collected describing both the physiological and physicochemical properties of supramolecular amphiphiles. Many of the techniques that are detailed throughout this review are incorporated within the flow chart in Fig. 25, including NMR spectroscopy (Section 1); HRMS (Section 2); SC-XRD (Section 4); CAC (Section 6); microscopy (Section 7); biological analysis (Section 8); and *in silico* modelling (Section 9).

This review has provided a substantial synopsis of identification, characterisation, and interactions of supramolecular amphiphiles using the most relevant techniques. An authoritative account of advantages and limitations of each method were discussed, and this detailed information was then supported by relevant case studies where suitable. The characterisation methods overviewed in this document are continually evolving, enabling improved analysis for these systems.

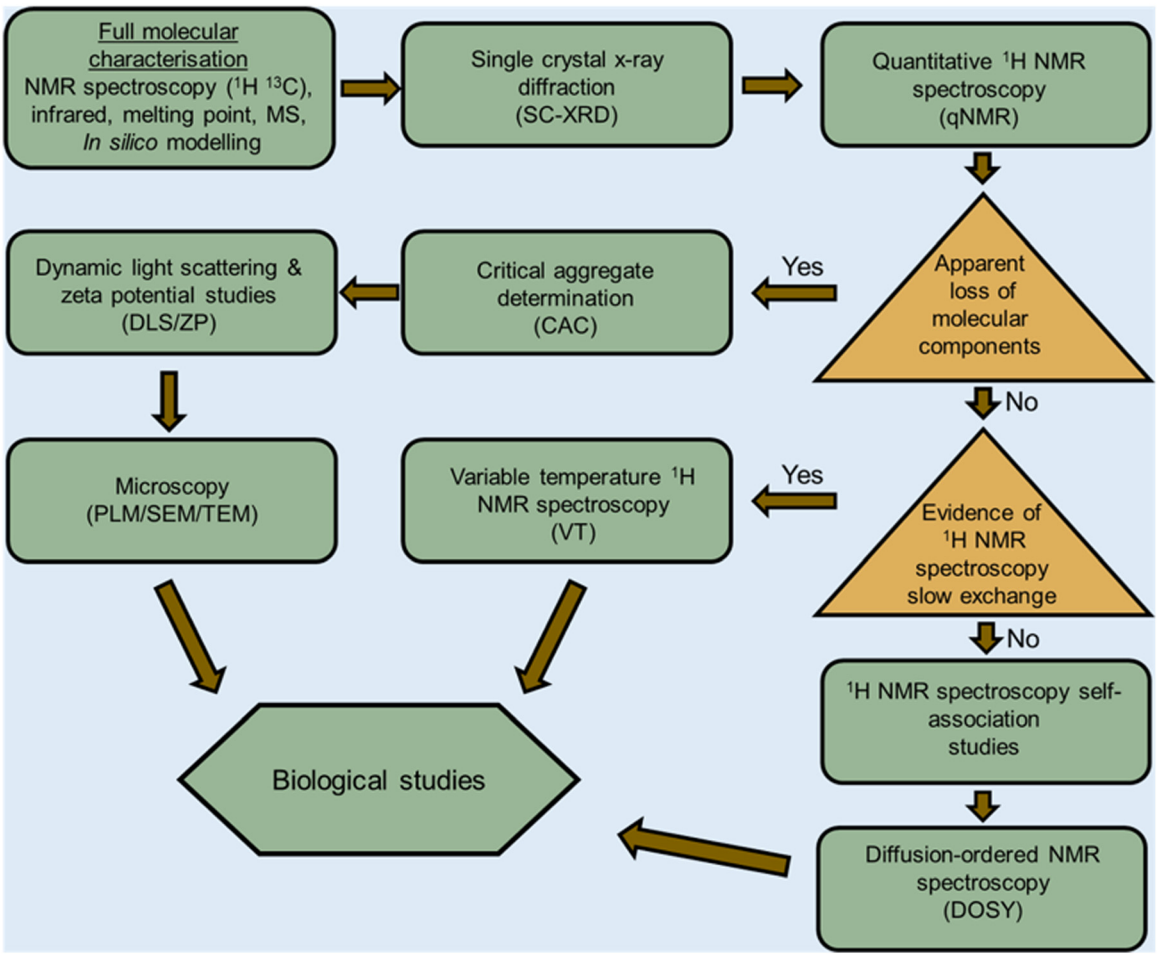

Fig. 25 Systematic method for the characterisation of SSAs.[11,15,34,36,37,41,47,48,181,182] Rectangle/hexagon = action; triangle = decision. Reproduced/adapted from ref.15 with permission from MDPI *Molecules*.

Each of these methods have their limitations which include, but are not limited to, physical state, sample size, and readily available information (software/knowledge). However, each independent method is a crucial piece of the puzzle towards the structural understanding of intra- or intermolecular interaction information, necessary for the characterisation of supramolecular amphiphilic systems. As such, each technique is best served as a key fragment used in conjunction with other techniques to give a full and comprehensive characterisation data set. It is our hope that this review both facilitates and inspires the analysis of supramolecular amphiphiles, and unlocks the limitless potential this sub-field of supramolecular chemistry has to offer to the wider scientific community.

Author contributions

TA, DEB, MKC, KLFH, OBK, RJL, CM, AO, PIAP, LRT, LJW: investigation; validation; writing – original draft, review & editing, CKH: reviewing; editing & supervision. JRH: conceptualization; funding acquisition; project administration; supervision; writing – original draft, review & editing.

Conflicts of interest

There are no conflicts to declare.

Acknowledgements

The authors would like to thank Mariam Yacoub for her contribution towards making this review visually inclusive. TA would like to thank Prof. Jeremy Frey (University of Southampton), Prof. J. Mark Sutton (UKHSA) for PhD funding and supervisory support. RJL would like to thank Prof. Claire Peppiatt-Wildman (University of Kent) for supervisory support. CM, PIAP, OBK and LRT would like to thank Prof. Michelle Garrett (University of Kent) for supervisory support. DB, KLFH, PIAP, AO, RJL, LRT and JRH would like to thank the University of Kent for funding. CM would like to thank the Jane Irons Scholarship for funding. OBK would like to thank the SoCoBio DTP for funding. LRT would like to thank the Daphne Jackson Trust, BBSRC, AstraZeneca, UKHSA and Cancer Research Horizons for funding and support. LJW and JRH would like to thank the UKRI (MR/T020415/1) for funding.

References

1 D. Lombardo, M. A. Kiselev, S. Magazù and P. Calandra, *Adv. Condens. Matter Phys.*, 2015, **2015**, 1–22.
2 N. O. Dora, E. Blackburn, J. E. Boles, G. T. Williams, L. J. White, S. E. G. Turner, J. D. Hothersall, T. Askwith, J. A. Doolan, D. P. Mulvihill, M. D. Garrett and J. R. Hiscock, *RSC Adv.*, 2021, **11**, 14213–14217.
3 J. E. Boles, C. Bennett, J. Baker, K. L. F. Hilton, H. A. Kotak, E. R. Clark, Y. Long, L. J. White, H. Y. Lai, C. K. Hind, J. M. Sutton, M. D. Garrett, A. Cheasty, J. L. Ortega-Roldan, M. Charles, C. J. E. Haynes and J. R. Hiscock, *Chem. Sci.*, 2022, **13**, 9761–9773.
4 N. Feiner-Gracia, M. Buzhor, E. Fuentes, S. Pujals, R. J. Amir and L. Albertazzi, *J. Am. Chem. Soc.*, 2017, **139**, 16677–16687.
5 K. L. F. Hilton, A. A. Karamalegkos, N. Allen, L. Gwynne, B. Streather, L. J. White, K. B. Baker, S. A. Henry, G. T. Williams, H. J. Shepherd, M. Shepherd, C. K. Hind, M. J. Sutton, T. A. Jenkins, D. P. Mulvihill, J. M. A. Tullet, M. Ezcurra and J. R. Hiscock, *J. Mater. Chem. B*, 2023, **11**, 3958–3968.
6 S. Song, A. Song and J. Hao, *RSC Adv.*, 2014, **4**, 41864–41875.
7 T. Guitton-Spassky, F. Junge, A. K. Singh, B. Schade, K. Achazi, M. Maglione, S. Sigrist, R. Rashmi and R. Haag, *Nanoscale*, 2023, **15**, 7781–7791.
8 L. Li, Z. Li, T. Balle, G. Liu and Z. Guo, *Food Hydrocolloids*, 2023, **139**, 108574.
9 D. Schwiertz, R. Holm and M. Barz, *Polym. J.*, 2020, **52**, 119–132.
10 P. Groves, *Polym. Chem.*, 2017, **8**, 6700–6708.
11 L. J. White, N. J. Wells, L. R. Blackholly, H. J. Shepherd, B. Wilson, G. P. Bustone, T. J. Runacres and J. R. Hiscock, *Chem. Sci.*, 2017, **8**, 7620–7630.
12 K. Hussain, A. Jabbar, K. Ali Hasan, M. Ali, Z. Ul-Haq, M. R. Shah, S. Ahmad Khan, M. A. Rashid, M. Kazi and M. N. Abbas, *Drug Delivery*, 2023, **30**, 2174205.
13 T. Guitton-Spassky, F. Junge, A. K. Singh, B. Schade, K. Achazi, M. Maglione, S. Sigrist, R. Rashmi and R. Haag, *Nanoscale*, 2023, **15**, 7781–7791.
14 P. Singh, P. Sharma, N. Sharma and S. Kaur, *J. Mater. Chem. B*, 2021, **10**, 107–119.
15 L. J. White, J. E. Boles, K. L. F. Hilton, R. J. Ellaby and J. R. Hiscock, *Molecules*, 2020, **25**, 4126.
16 A. M. Peterson, Z. Tan, E. M. Kimbrough and J. M. Heemstra, *Anal. Methods*, 2015, **7**, 6877–6882.
17 J. W. Steed, D. R. Turner and K. J. Wallace, *Core Concepts in Supramolecular Chemistry and Nanochemistry*, John Wiley & Sons, Hoboken, 1st edn, 2007.
18 J.-M. Lehn, *Chem. Soc. Rev.*, 2007, **36**, 151–160.
19 X. Zhang and C. Wang, *Chem. Soc. Rev.*, 2011, **40**, 94–101.
20 J. Liu, M. Morikawa and N. Kimizuka, *J. Am. Chem. Soc.*, 2011, **133**, 17370–17374.
21 G. Schwarz, Y. Bodenthin, Z. Tomkowicz, W. Haase, T. Geue, J. Kohlbrecher, U. Pietsch and D. G. Kurth, *J. Am. Chem. Soc.*, 2011, **133**, 547–558.
22 B. Reif, S. E. Ashbrook, L. Emsley and M. Hong, *Nat. Rev. Methods Primers*, 2021, **1**, 2.
23 R. W. Hooper, D. Sarkar and V. K. Michaelis, *Curr. Opin. Colloid Interface Sci.*, 2022, **62**, 101631.
24 W. P. Power, *Annu. Rep. NMR Spectrosc.*, 2011, **72**, 111–156.
25 M. Pellecchia, *Chem. Biol.*, 2005, **12**, 961–971.
26 M. Monduzzi and B. Lindman, *Curr. Opin. Colloid Interface Sci.*, 2019, **44**, 14–22.
27 M. P. Foster, C. A. McElroy and C. D. Amero, *Biochemistry*, 2007, **46**, 331–340.
28 X. Liu, Q. Yu, A. Song, S. Dong and J. Hao, *Curr. Opin. Colloid Interface Sci.*, 2020, **45**, 14–27.

29 E. Bednarek, W. Bocian and K. Michalska, *J. Pharm. Biomed. Anal.*, 2019, **169**, 170–180.
30 A. Che, C. O. Zellman, D. Sarkar, S. Trudel-Lachance, J. Espejo, V. K. Michaelis, V. E. Williams and C.-C. Ling, *J. Mater. Chem. C*, 2023, **11**, 4153–4163.
31 T. Polenova, R. Gupta and A. Goldbourt, *Anal. Chem.*, 2015, **87**, 5458–5469.
32 P. C. A. van der Wel, *Emerging Top. Life Sci.*, 2018, **2**, 57–67.
33 M. Auger, *Curr. Issues Mol. Biol.*, 2000, **2**, 119–124.
34 N. Allen, L. J. White, J. E. Boles, G. T. Williams, D. F. Chu, R. J. Ellaby, H. J. Shepherd, K. K. L. Ng, L. R. Blackholly, B. Wilson, D. P. Mulvihill and J. R. Hiscock, *ChemMedChem*, 2020, **15**, 2193–2205.
35 J. Wang, X. Ding and X. Guo, *Adv. Colloid Interface Sci.*, 2019, **269**, 187–202.
36 A. Rutkauskaite, L. J. White, J. E. Boles, K. L. F. Hilton, M. Clifford, B. Patenall, B. R. Streather, D. P. Mulvihill, S. A. Henry, M. Shepherd, J. M. Sutton, C. K. Hind and J. R. Hiscock, *Supramol. Chem.*, 2021, **33**, 677–686.
37 J. E. Boles, G. T. Williams, N. Allen, L. J. White, K. L. F. Hilton, P. I. A. Popoola, D. P. Mulvihill and J. R. Hiscock, *Adv. Ther.*, 2022, **5**, 2200024.
38 P. Thordarson, *Chem. Soc. Rev.*, 2011, **40**, 1305–1323.
39 L. K. S. von Krbek, C. A. Schalley and P. Thordarson, *Chem. Soc. Rev.*, 2017, **46**, 2622–2637.
40 Supramolecular.org - Binding Constant Calculators | Supramolecular, **https://app.supramolecular.org/bindfit/**, [accessed 1 May 2023].
41 L. R. Blackholly, H. J. Shepherd and J. R. Hiscock, *CrystEngComm*, 2016, **18**, 7021–7028.
42 R. B. Martin, *Chem. Rev.*, 1996, **96**, 3043–3064.
43 P. R. Stoesser and S. J. Gill, *J. Phys. Chem.*, 1967, **71**, 564–567.
44 N. Busschaert, C. Caltagirone, W. Van Rossom and P. A. Gale, *Chem. Rev.*, 2015, **115**, 8038–8155.
45 P. A. Gale and C. Caltagirone, *Chem. Soc. Rev.*, 2015, **44**, 4212–4227.
46 C. M. C. Faustino, A. R. T. Calado and L. Garcia-Rio, *J. Phys. Chem. B*, 2009, **113**, 977–982.
47 J. E. Boles, R. J. Ellaby, H. J. Shepherd and J. R. Hiscock, *RSC Adv.*, 2021, **11**, 9550–9556.
48 L. J. White, S. N. Tyuleva, B. Wilson, H. J. Shepherd, K. K. L. Ng, S. J. Holder, E. R. Clark and J. R. Hiscock, *Chem. – Eur. J.*, 2018, **24**, 7761–7773.
49 M. A. Geer Wallace and J. P. McCord, *Breathborne Biomarkers Hum*, Elsevier, Volatilome, 2nd edn, 2020, pp. 253–270.
50 E. Geddes da Filicaia, R. P. Evershed and D. A. Peggie, *Anal. Chim. Acta*, 2023, **1246**, 340575.
51 A. G. Cheetham, Y. Lin, R. Lin and H. Cui, *Acta Pharmacol. Sin.*, 2017, **38**, 874–884.
52 V. Burilov, D. Mironova, E. Sultanova, R. Garipova, V. Evtugyn, S. Solovieva and I. Antipin, *Molecules*, 2021, **26**, 6864.
53 L. Polewski, A. Springer, K. Pagel and C. A. Schalley, *Acc. Chem. Res.*, 2021, **54**, 2445–2456.
54 H. Wang, C. Guo and X. Li, *CCS Chem.*, 2022, **4**, 785–808.
55 A. El-Aneed, A. Cohen and J. Banoub, *Appl. Spectrosc. Rev.*, 2009, **44**, 210–230.
56 E. A. Andreyko, P. L. Padnya and I. I. Stoikov, *Colloids Surf., A*, 2014, **454**, 74–83.
57 Y. Shao, J. Chen, X.-K. Ren, X. Zhang, G.-Z. Yin, X. Li, J. Wang, C. Wesdemiotis, W.-B. Zhang, S. Yang, B. Sun and M. Zhu, *Molecules*, 2019, **24**, 2114.
58 J. Mei, Y. Hong, J. W. Y. Lam, A. Qin, Y. Tang and B. Z. Tang, *Adv. Mater.*, 2014, **26**, 5429–5479.
59 S. Tencé-Girault, S. Lebreton, O. Bunau, P. Dang and F. Bargain, *Crystals*, 2019, **9**, 271.
60 J. Crawshaw, W. Bras, G. R. Mant and R. E. Cameron, *J. Appl. Polym. Sci.*, 2002, **83**, 1209–1218.
61 M. K. Pradhan, D. Gupta, K. R. Namdev, N. Anjali, C. Miglani, A. Pal and A. Srivastava, *Nanoscale*, 2022, **14**, 15079–15090.
62 D. A. Mannock, M. D. Collins, M. Kreichbaum, P. E. Harper, S. M. Gruner and R. N. McElhaney, *Chem. Phys. Lipids*, 2007, **148**, 26–50.
63 M. C. Lin, C. H. Hsu, H. J. Sun, C. L. Wang, W. B. Zhang, Y. Li, H. L. Chen and S. Z. D. Cheng, *Polymer*, 2014, **55**, 4514–4520.
64 H. J. Sun, Y. Tu, C. L. Wang, R. M. Van Horn, C. C. Tsai, M. J. Graham, B. Sun, B. Lotz, W. Bin Zhang and S. Z. D. Cheng, *J. Mater. Chem.*, 2011, **21**, 14240–14247.
65 Y. Alqaheem and A. A. Alomair, *Membranes*, 2020, **10**, 33.
66 B. Bhat, S. Pahari, S. Liu, Y. T. Lin, J. S. I. Kwon and M. Akbulut, *Colloids Surf., A*, 2022, **654**, 130067.
67 A. S. Weingarten, R. V. Kazantsev, L. C. Palmer, D. J. Fairfield, A. R. Koltonow and S. I. Stupp, *J. Am. Chem. Soc.*, 2015, **137**, 15241–15246.
68 K. Hasegawa, *Rigaku J.*, 2012, **28**, 14–18.
69 B. Dittrich, J. Lübben, S. Mebs, A. Wagner, P. Luger and R. Flaig, *Chem. – Eur. J.*, 2017, **23**, 4605–4614.
70 D. Ishii, T. Yamada, M. Nakagawa, T. Iyoda and H. Yoshida, *J. Therm. Anal. Calorim.*, 2006, **86**, 681–685.
71 T. W. Martin and Z. S. Derewenda, *Nat. Struct. Mol. Biol.*, 1999, **6**, 403–406.
72 A. Manikandan, M. Dhanalakshmi, L. Guganathan, T. Kokila, M. Santhamoorthy, R. Markkandan, S. C. Kim and C. Balakrishnan, *J. Mol. Struct.*, 2022, **1254**, 132395.
73 B. A. Nogueira, C. Castiglioni and R. Fausto, *Commun. Chem.*, 2020, **3**, 34.
74 M. Pitak, Exploring the advantages of single-crystal X-ray diffraction in pharma, **https://www.chemistryworld.com/sponsored-content/exploring-the-advantages-of-single-crystal-X-ray-diffraction-in-pharma/4012282.article**, [accessed 23 May 2023].
75 Y. Zhao, Y. Lu, A. Liu, Z. Y. Zhang, C. Li and A. C. H. Sue, *Molecules*, 2023, **28**, 2537.
76 M. Douzapau, S. Roy Chowdhury, S. Singh, O. J. Ibukun and D. Haldar, *Chemistry*, 2023, **5**, 691–702.
77 C. Po, A. Y. Y. Tam, K. M. C. Wong and V. W. W. Yam, *J. Am. Chem. Soc.*, 2011, **133**, 12136–12143.

78 N. Liu, B. Wang, W. Liu and W. Bu, *J. Mater. Chem. C*, 2013, **1**, 1130–1136.
79 B. Song, G. Wu, Z. Wang, X. Zhang, M. Smet and W. Dehaen, *Langmuir*, 2009, **25**, 13306–13310.
80 F. Wang, M. Lan, W. P. To, K. Li, C. N. Lok, P. Wang and C. M. Che, *Chem. Commun.*, 2016, **52**, 13273–13276.
81 F. Tosi, M. C. A. Stuart, S. J. Wezenberg and B. L. Feringa, *Angew. Chem.*, 2019, **58**, 14935–14939.
82 P. Schuck, *Biophys. J.*, 2000, **78**, 1606–1619.
83 J. Lebowitz, M. S. Lewis and P. Schuck, *Protein Sci.*, 2009, **11**, 2067–2079.
84 M. Raşa and U. S. Schubert, *Soft Matter*, 2006, **2**, 561–572.
85 B. G. G. Lohmeijer and U. S. Schubert, *Angew. Chem.*, 2002, **41**, 3825–3829.
86 J. F. Gohy, B. G. G. Lohmeijer and U. S. Schubert, *Macromolecules*, 2002, **35**, 4560–4563.
87 J. F. Gohy, B. G. G. Lohmeijer, B. Décamps, E. Leroy, S. Boileau, J. A. van den Broek, D. Schubert, W. Haase and U. S. Schubert, *Polym. Int.*, 2003, **52**, 1611–1618.
88 O. Regev, J. F. Gohy, B. G. G. Lohmeijer, S. K. Varshney, D. H. W. Hubert, P. M. Frederik and U. S. Schubert, *Colloid Polym. Sci.*, 2004, **282**, 407–411.
89 V. Vogel, J. F. Gohy, B. G. G. Lohmeijer, J. A. Van Den Broek, W. Haase, U. S. Schubert and D. Schubert, *J. Polym. Sci., Part A: Polym. Chem.*, 2003, **41**, 3159–3168.
90 G. Mayer, V. Vogel, B. G. G. Lohmeijer, J. F. Gohy, J. A. Van Den Broek, W. Haase, U. S. Schubert and D. Schubert, *J. Polym. Sci., Part A: Polym. Chem.*, 2004, **42**, 4458–4465.
91 S. S. Andrews and J. Tretton, *J. Chem. Educ.*, 2020, **97**, 4370–4376.
92 A. J. Miles and B. A. Wallace, *Chem. Soc. Rev.*, 2016, **45**, 4859–4872.
93 S. Bayindir, K. S. Lee, N. Saracoglu and J. R. Parquette, *Dalton Trans.*, 2020, **49**, 13685–13692.
94 V. Mittal, A. Völkel and H. Cölfen, *Macromol. Biosci.*, 2010, **10**, 754–762.
95 M. J. Rosen and J. T. Kunjappu, *Surfactants and Interfacial Phenomena*, John Wiley & Sons, Hoboken, 4th edn, 2012, vol. 4.
96 B. E. Rapp, *Microfluidics: Modelling, Mechanics and Mathematics*, Elsevier, Amsterdam, 2017, pp. 453–465.
97 H. J. Butt, K. Graf and M. Kappl, *Physics and Chemistry of Interfaces*, John Wiley & Sons, Hoboken, 1st edn, 2003.
98 J. D. Berry, M. J. Neeson, R. R. Dagastine, D. Y. C. Chan and R. F. Tabor, *J. Colloid Interface Sci.*, 2015, **454**, 226–237.
99 E. Mohajeri and G. Dehghan, *Eur. J. Chem.*, 2012, **9**, 2268–2274.
100 A. Patist, S. S. Bhagwat, K. W. Penfield, P. Aikens and D. O. Shah, *J. Surfactants Deterg.*, 2000, **3**, 53–58.
101 C. S. Buettner, A. Cognigni, C. Schröder and K. Bica-Schröder, *J. Mol. Liq.*, 2022, **347**, 118160.
102 K. P. Ananthapadmanabhan, E. D. Goddard, N. J. Turro and P. L. Kuos, *Langmuir*, 1985, **1**, 352–355.
103 G. Nizri and S. Magdassi, *J. Colloid Interface Sci.*, 2005, **291**, 169–174.
104 I. N. Kurniasih, H. Liang, P. C. Mohr, G. Khot, J. P. Rabe and A. Mohr, *Langmuir*, 2015, **31**, 2639–2648.
105 M. G. Cottingham, C. D. Bain and D. J. T. Vaux, *Lab. Invest.*, 2004, **84**, 523–529.
106 L. Cai and M. Gochin, *SLAS Discovery*, 2007, **12**, 966–971.
107 L. Cai, M. Gochin and K. Liu, *Chem. Commun.*, 2011, **47**, 5527–5529.
108 A. Rutkauskaite, L. J. White, K. L. F. Hilton, G. Picci, L. Croucher, C. Caltagirone and J. R. Hiscock, *Org. Biomol. Chem.*, 2022, **20**, 5999–6006.
109 R. A. Al-Juboori and T. Yusaf, *Desalination*, 2012, **302**, 1–23.
110 G. Pompeo, M. Girasole, A. Cricenti, F. Cattaruzza, A. Flamini, T. Prosperi, J. Generosi and A. Congiu Castellano, *Biochim. Biophys. Acta, Biomembr.*, 2005, **1712**, 29–36.
111 Q. Rao, H. Wang, X. Fan and Y. Zhou, *Rare Met. Mater. Eng.*, 2003, **32**, 420–423.
112 M. Aliofkhazraei and N. Ali, in *Comprehensive Materials Processing*, ed. S. Hashmi, G. F. Batalha, C. J. Van Tyne and B. Yilbas, Elsevier, Amsterdam, 2014, vol. 7, pp. 191–241.
113 S. Han, W. Xu, C. Meiwen, W. Jiqian, D. Xia, H. Xu, X. Zhao and J. R. Lu, *Soft Matter*, 2012, **8**, 645–652.
114 G. C. Feast, O. E. Hutt, X. Mulet, C. E. Conn, C. J. Drummond and G. P. Savage, *Chem. – Eur. J.*, 2014, **20**, 2783–2792.
115 G. C. Feast, T. Lepitre, X. Mulet, C. E. Conn, O. E. Hutt, G. P. Savage and C. J. Drummond, *Beilstein J. Org. Chem.*, 2014, **10**, 1578–1588.
116 J. W. Lichtman and J. A. Conchello, *Nat. Methods*, 2005, **2**, 910–919.
117 L. J. White, J. E. Boles, N. Allen, L. S. Alesbrook, J. M. Sutton, C. K. Hind, K. L. F. Hilton, L. R. Blackholly, R. J. Ellaby, G. T. Williams, D. P. Mulvihill and J. R. Hiscock, *J. Mater. Chem. B*, 2020, **8**, 4694–4700.
118 S. J. Pennycook, *Encyclopedia of Condensed Matter Physics*, Elsevier, Amsterdam, 2005, pp. 240–247.
119 J. M. Ludlow, M. J. Saunders, M. Huang, Z. Guo, C. N. Moorefield, S. Z. D. Cheng, C. Wesdemiotis and G. R. Newkome, *Supramol. Chem.*, 2017, **29**, 69–79.
120 J. Huang, P. Wu, S. Dong and B. Gao, *Emerging Contaminants in Soil and Groundwater Systems*, Elsevier, Amsterdam, 2022, pp. 253–299.
121 L. Latxague, A. Gaubert and P. Barthélémy, *Molecules*, 2018, **23**, 89.
122 C. Yang, Z. Song, J. Zhao, Z. Hu, Y. Zhang and Q. Jiang, *Colloids Surf., A*, 2017, **523**, 62–70.
123 M. E. Cano, P. H. Di Chenna, D. Lesur, A. Wolosiuk, J. Kovensky and M. L. Uhrig, *New J. Chem.*, 2017, **41**, 14754–14765.
124 O. P. Choudhary and P. Choudhary, *Int. J. Curr. Microbiol. Appl. Sci.*, 2017, **6**, 1877–1882.
125 B. R. Denzer, R. J. Kulchar, R. B. Huang and J. Patterson, *Gels*, 2021, **7**, 158.
126 J. L. S. Milne, M. J. Borgnia, A. Bartesaghi, E. E. H. Tran, L. A. Earl, D. M. Schauder, J. Lengyel, J. Pierson, A. Patwardhan and S. Subramaniam, *FEBS J.*, 2013, **280**, 28–45.
127 Z. Kochovski, G. Chen, J. Yuan and Y. Lu, *Colloid Polym. Sci.*, 2020, **298**, 707–717.

128 H. Cui, T. K. Hodgdon, E. W. Kaler, L. Abezgauz, D. Danino, M. Lubovsky, Y. Talmon and D. J. Pochan, *Soft Matter*, 2007, **3**, 945.
129 M. R. Leung and T. Zeev-Ben-Mordehai, *J. Neurochem.*, 2021, **158**, 1236–1243.
130 A. J. Higgins, A. J. Flynn, A. Marconnet, L. J. Musgrove, V. L. G. Postis, J. D. Lippiat, C. Chung, T. Ceska, M. Zoonens, F. Sobott and S. P. Muench, *Commun. Biol.*, 2021, **4**, 1337.
131 K. Mio and C. Sato, *Biophys. Rev.*, 2018, **10**, 307–316.
132 A. L. Parry, P. H. H. Bomans, S. J. Holder, N. A. J. M. Sommerdijk and S. C. G. Biagini, *Angew. Chem.*, 2008, **47**, 8859–8862.
133 P. Workman and I. Collins, *Chem. Biol.*, 2010, **17**, 561–577.
134 M. Bin Samad, K. Maddeboina, N. Rodrigues de Almeida and M. Conda-Sheridan, *J. Visualized Exp.*, 2018, e57908.
135 S. Chen, R. Costil, F. K. Leung and B. L. Feringa, *Angew. Chem.*, 2021, **60**, 11604–11627.
136 P. Saraf, X. Li, L. Wrischnik and B. Jasti, *Pharm. Res.*, 2015, **32**, 3087–3101.
137 A. Brito, S. Kassem, R. L. Reis, R. V. Ulijn, R. A. Pires and I. Pashkuleva, *Chem.*, 2021, **7**, 2943–2964.
138 B. Parshad, S. Prasad, S. Bhatia, A. Mittal, Y. Pan, P. K. Mishra, S. K. Sharma and L. Fruk, *RSC Adv.*, 2020, **10**, 42098–42115.
139 L. Di and E. Kerns, *Chem. Biodiversity*, 2009, **6**, 1875–1886.
140 Y. Lu, E. Zhang, J. Yang and Z. Cao, *Nano Res.*, 2018, **11**, 4985–4998.
141 M. Haikola, J. Hirvonen, O. Penate Medina, I. Simpura, K. Kairemo and L. Peltonen, *J. Drug Delivery Sci. Technol.*, 2011, **21**, 183–188.
142 P. Xing and Y. Zhao, *Adv. Mater.*, 2016, **28**, 7304–7339.
143 Y. S. Lee, *Self-Assembly and Nanotechnology*, Wiley, 2008.
144 K. Morigaki and P. Walde, *Curr. Opin. Colloid Interface Sci.*, 2007, **12**, 75–80.
145 M. Bergmeier, M. Gradzielski, H. Hoffmann and K. Mortensen, *J. Phys. Chem. B*, 1998, **102**, 2837–2840.
146 J.-F. Berret, D. C. Roux and G. Porte, *J. Phys. II*, 1994, **4**, 1261–1279.
147 P. Brown, C. P. Butts and J. Eastoe, *Soft Matter*, 2013, **9**, 2365.
148 T. Stylianopoulos and R. K. Jain, *Nanomedicine*, 2015, **11**, 1893–1907.
149 C. A. Lipinski, F. Lombardo, B. W. Dominy and P. J. Feeney, *Adv. Drug Delivery Rev.*, 2001, **46**, 3–26.
150 M. Yang and W. J. Brackenbury, *Front. Physiol.*, 2013, **4**, 1–10.
151 M. C. Frantz and P. Wipf, *Environ. Mol. Mutagen.*, 2010, **51**, 462–475.
152 M. T. Jeena, L. Palanikumar, E. M. Go, I. Kim, M. G. Kang, S. Lee, S. Park, H. Choi, C. Kim, S. M. Jin, S. C. Bae, H. W. Rhee, E. Lee, S. K. Kwak and J. H. Ryu, *Nat. Commun.*, 2017, **8**, 26.
153 D. J. Kim, M. T. Jeena, O. H. Kim, H. E. Hong, H. Seo, J. H. Ryu and S. J. Kim, *Int. J. Mol. Sci.*, 2020, **21**, 6126.
154 M. T. Jeena, S. Jin, B. Jana and J. H. Ryu, *RSC Chem. Biol.*, 2022, **3**, 1416–1421.
155 Y. Lu, Z. Yue, J. Xie, W. Wang, H. Zhu, E. Zhang and Z. Cao, *Nat. Biomed. Eng.*, 2018, **2**, 318–325.
156 H. Su, F. Wang, W. Ran, W. Zhang, W. Dai, H. Wang, C. F. Anderson, Z. Wang, C. Zheng, P. Zhang, Y. Li and H. Cui, *Proc. Natl. Acad. Sci. U. S. A.*, 2020, **117**, 4518–4526.
157 D. K. Ho, R. Christmann, X. Murgia, C. De Rossi, S. Frisch, M. Koch, U. F. Schaefer, B. Loretz, D. Desmaele, P. Couvreur and C. M. Lehr, *Front. Chem.*, 2020, **8**, 584242.
158 L. Li, R. Sun and R. Zheng, *Mater. Des.*, 2021, **197**, 109209.
159 B. O. Okesola, Y. Wu, B. Derkus, S. Gani, D. Wu, D. Knani, D. K. Smith, D. J. Adams and A. Mata, *Chem. Mater.*, 2019, **31**, 7883–7897.
160 V. V. Acuna, R. M. Hopper and R. J. Yoder, *J. Chem. Educ.*, 2020, **97**, 760–763.
161 C. Y. Jia, J. Y. Li, G. F. Hao and G. F. Yang, *Drug Discovery Today*, 2020, **25**, 248–258.
162 F. Wu, Y. Zhou, L. Li, X. Shen, G. Chen, X. Wang, X. Liang, M. Tan and Z. Huang, *Front. Chem.*, 2020, **8**, 1–32.
163 N. Pillai, A. Dasgupta, S. Sudsakorn, J. Fretland and P. D. Mavroudis, *Drug Discovery Today*, 2022, **27**, 2209–2215.
164 S. Q. Pantaleão, P. O. Fernandes, J. E. Gonçalves, V. G. Maltarollo and K. M. Honorio, *ChemMedChem*, 2022, **17**, e202100542.
165 J. Dulsat, B. López-Nieto, R. Estrada-Tejedor and J. I. Borrell, *Molecules*, 2023, **28**, 776.
166 A. Daina, O. Michielin and V. Zoete, *Sci. Rep.*, 2017, **7**, 42717.
167 J. Dong, N.-N. Wang, Z.-J. Yao, L. Zhang, Y. Cheng, D. Ouyang, A.-P. Lu and D.-S. Cao, *J. Cheminf.*, 2018, **10**, 29.
168 G. Xiong, Z. Wu, J. Yi, L. Fu, Z. Yang, C. Hsieh, M. Yin, X. Zeng, C. Wu, A. Lu, X. Chen, T. Hou and D. Cao, *Nucleic Acids Res.*, 2021, **49**, W5–W14.
169 D. Lagorce, L. Bouslama, J. Becot, M. A. Miteva and B. O. Villoutreix, *Bioinformatics*, 2017, **33**, 3658–3660.
170 P. L. Scognamiglio, C. Riccardi, R. Palumbo, T. F. Gale, D. Musumeci and G. N. Roviello, *J. Nanostruct. Chem.*, 2023, 1–19.
171 W. Zou, A. Martell Monterroza, Y. Yao, S. C. Millik, M. M. Cencer, N. J. Rebello, H. K. Beech, M. A. Morris, T.-S. Lin, C. S. Castano, J. A. Kalow, S. L. Craig, A. Nelson, J. S. Moore and B. D. Olsen, *Chem. Sci.*, 2022, **13**, 12045–12055.
172 S. Rahal, N. Hadidi and M. Hamadache, *Arabian J. Sci. Eng.*, 2020, **45**, 7445–7454.
173 E. N. Muratov, J. Bajorath, R. P. Sheridan, I. V. Tetko, D. Filimonov, V. Poroikov, T. I. Oprea, I. I. Baskin, A. Varnek, A. Roitberg, O. Isayev, S. Curtalolo, D. Fourches, Y. Cohen, A. Aspuru-Guzik, D. A. Winkler, D. Agrafiotis, A. Cherkasov and A. Tropsha, *Chem. Soc. Rev.*, 2020, **49**, 3525–3564.
174 A. Mozrzymas, *J. Solution Chem.*, 2013, **42**, 2187–2199.
175 M. Jalali-Heravi and E. Konouz, *J. Surfactants Deterg.*, 2003, **6**, 25–30.
176 RDKit: Open-source cheminformatics, **https://www.rdkit.org**. [accessed 3 May 2023].
177 M. Turchi, A. P. Karcz and M. P. Andersson, *J. Colloid Interface Sci.*, 2022, **606**, 618–627.

178 R. Van Lommel, J. Zhao, W. M. De Borggraeve, F. De Proft and M. Alonso, *Chem. Sci.*, 2020, **11**, 4226–4238.
179 P. Mukerjee and K. J. Mysels, *Critical Micelle Concentrations of Aqueous Surfactant Systems*, US government printing office, 1971, 36.
180 J. Thomas, M. Navre, A. Rubio and A. Coukell, *ACS Infect. Dis.*, 2018, **4**, 1536–1539.
181 L. J. White, J. E. Boles, M. Clifford, B. L. Patenall, K. H. L. F. Hilton, K. K. L. Ng, R. J. Ellaby, C. K. Hind, D. P. Mulvihill and J. R. Hiscock, *Chem. Commun.*, 2021, **57**, 11839–11842.
182 S. N. Tyuleva, N. Allen, L. J. White, A. Pépés, H. J. Shepherd, P. J. Saines, R. J. Ellaby, D. P. Mulvihill and J. R. Hiscock, *Chem. Commun.*, 2019, **55**, 95–98.